CDF/ANAL/EXOTIC/CDFR/7237

Search for the Quasi-Stable Doubly-Charged Higgs in 292 pb^{-1}

Joshua Tuttle, Ashutosh Kotwal, and Chris Hays
Duke University

December 25, 2004

Abstract

We describe the inclusion of an additional 90 pb^{-1} of data to our search for a long-lived doubly-charged Higgs particle [4] in CDF Run 2. Our search now uses $(292.0 \pm 16.6)pb^{-1}$ of high p_T muon data taken between February, 2002 and February, 2004. After finding 0 candidate particles, we set a mass limit of 146 GeV on quasi-stable $H^{\pm\pm}$ production.

1 Introduction

In previous notes [1, 2, 3] searches for doubly-charged particles in dielectron, dimuon, and electron-muon data respectively were described. We extend this search to the case of no intra-detector decay ($c\tau > 3$m) of the doubly-charged particle in [4]. We demonstrated our cut optimization in [5]. We also describe our decision to divide the search into a "loose" search (for setting limits) and a "tight" search (for claiming discovery). We use the doubly-charged Higgs model to calculate the detector acceptance. The phenomenology of these particles can be found in [1].

1.1 Dataset

We use $\sim 290\ pb^{-1}$ of data collected between February, 2002 and February, 2004. The datasets our signal sample is taken from are `bhmu08` and `bhmu09`. The sample is separated into runs with both the CMUP and CMX, the CMUP only, and the CMX only. We use good run lists compiled by Chris Hays [11] using the CDF e-logs and the COT and calorimeter good run lists. We analyze $((250.9 \pm 14.3)\ pb^{-1})$ of data from the runs with both CMUP and CMX, $((32.1 \pm 1.8)\ pb^{-1})$ using CMUP only, and $((9.0 \pm 0.5)\ pb^{-1})$ using the CMX only. The data are processed using CdfSoftware version 5.3.1 full post-production processing.

2 Ionization

Massive charged particles traveling post-collision through the CDF detector primarily lose energy due to ionization. Ionization produced by these particles is given by the Bethe-Bloch equation [7]:

$$-\frac{dE}{dx} = Kz^2\frac{Z}{A}\frac{1}{\beta^2}[\frac{1}{2}\ln(\frac{2m_ec^2\beta^2\gamma^2T_{max}}{I^2}) - \beta^2 - \frac{\delta}{2}], \tag{1}$$

where z is the charge of the incident particle.

Since the ionization of a particle is proportional to the square of its charge, a doubly-charged particle would cause four times the ionization of a singly-charged one. We exploit this large difference in ionization in our search for a long-lived doubly-charged Higgs.

2.1 Measurement of Ionization

Energy loss due to ionization can be measured several different ways within the CDF detector. We employ the combined dE/dx measurements of calorimeters and tracking devices to get a complete picture of a particle's ionization.

Both the hadronic and electromagnetic calorimeters measure dE/dx for minimum-ionizing particles. We use the transverse component of these energy-depositions as recorded by each calorimeter along the track of the particle whose ionization we seek to measure. We call these quantities $HadET$ and $EMET$ respectively.

The COT also encodes dE/dx information in the width of the pulse of each hit, and provides a particularly useful ionization measurement. In this analysis we use the COT dE/dx measurement calibrated at the hit-level by Eiko Yu *et.al* [8] and at the "macroscopic" run-level by members of the CDF bottom group [9] which we denote by the abbreviation $COTHW$.

2.2 Detector Mismeasurement of Ionization

Whether or not a particle can be considered highly ionizing based on its $HadET$, $EMET$, and $COTHW$ values is subject to detector effects. There are several detector and event characteristics that can contribute to mismeasurement of these variables and thus allow muons to occasionally mimic a highly ionizing particle.

It is statistically possible for a muon to occasionally give large values for each of the three measured dE/dx quantities. Other particles in close proximity to a muon can increase the apparent ionization produced by the muon. Thus, it is advantageous to use a combination of all three variables to eliminate many of these anamalous readings, thereby reducing the rate of muons mimicking highly ionizing particles.

In events with a large number of tracks or tracks very close together, real muon hits can become merged with other nearby hits thus increasing the pulse width recorded by $COTHW$. Studies of fake rate systematics in Section 5.2 illustrate the increase in fake highly ionizing muon events measured by $COTHW$ as the number of tracks in the COT increases.

The calorimeter can experience mismeasurement of $HadET$ and $EMET$ when underlying event or jet energy overlaps the muon towers being analyzed. Such an overlap could also allow the muon to be mislabeled as a highly ionizing particle.

3 Selection Criteria

There are three tables defining our cuts in this analysis. Table 1 gives both the Track Cuts and Stub Cuts referenced throughout, Table 2 gives the muon ID cuts which we use for counting the number of $Z \to \mu\mu$ events in the current data sample, and Table 3 gives the cuts we use for identification of a $H^{\pm\pm}$.

Variable	Cut
Track Cuts:	
$\|z_0\|$	< 60.0 cm
# Stereo hits	≥ 3 SL with ≥ 5 hits or COT layer < 96
# Axial hits	≥ 3 SL with ≥ 5 hits or COT layer < 96
$\|d_0\|$	< 0.2 cm
(isolation in R=0.4 cone)/p_T	< 0.1
p_T	> 20 GeV
ρ_{COT}	> 140 cm
Cosmic Ray Veto	
Stub Cuts:	
$\|\Delta x_{CMU}\|$	< 3.0 cm
$\|\Delta x_{CMP}\|$	< 5.0 cm
$\|\Delta x_{CMX}\|$	< 6.0 cm
Fiducial Muon	

Table 1: *Track Cuts and Stub Cuts used throughout the analysis.*

We define two separate sets of ionization cuts in our analysis. The loose cuts seek to maximize efficiency and are used exclusively for setting a mass limit. The tight cuts on the other hand are used to virtually eliminate the fake backgrounds and will be used only in case of discovery. Since the combined cuts on $EMET$ and $HadET$ are fairly inefficient, the ability to set a limit suffers when using them. Thus, Table 3 indicates we completely removed these cuts in our loose category.

Variable	Cut
Track Cuts	from Table 1
Stub Cuts	from Table 1
E_{em}	$< 2 + \max(0,(p - 100) \times 0.0115)$ GeV
E_{had}	$< 6 + \max(0,(p - 100) \times 0.0280)$ GeV

Table 2: *Muon ID cuts.*

Variable	Loose Cuts	Tight Cuts
EMET	no cut	> 0.6 GeV
HadET	no cut	> 4 GeV
COTHW	> 35 ns	> 35 ns

Table 3: *The three high ionization cuts used in identifying $H^{\pm\pm}$. We use the loose ionization cuts only for setting a limit, and the tight ionization cuts only for possible discovery of $H^{\pm\pm}$.*

Variable	Cut
Highly Ionizing Track with Stub	from Tables 1 & 3
Second Highly Ionizing Track	from Tables 1 & 3

Table 4: *$H^{\pm\pm}$ ID cuts.*

4 Efficiencies

4.1 Muon ID Efficiencies

We find the efficiency to identify muons using Z data by selecting events with two opposite-sign muon candidates having a reconstructed mass between 80 and 100 GeV. We require that one of these muons must pass the Track Cuts in Table 1, while the second is required to pass only the p_T, $|z_0|$, and ρ_{COT} cuts in that table and a looser cut on d_0 ($|d_0| < 1$ cm) while removing identified cosmics. From the resulting sample, we count events where the second muon passes all the Track Cuts (N_2) and also events where the second muon fails the Track Cuts (N_1). From these two numbers we calculate the efficiency of the Track Cuts to be:

$$\epsilon = \frac{2N_2}{2N_2 + N_1} \tag{2}$$

I similarly found the Trigger and Stub efficiencies for the CMUP and CMX detectors. Chris found the cosmic ray tagger to be 100% efficient, with an upper limit of 0.8% on the inefficiency [11]. Thus the cosmic tagger efficiency is considered to be $100.0^{+0.0}_{-0.8}$%. For the $|z_0|$ cut we used the efficiency given by the WZ cross section group [13].

I show this new efficiency for All Track Cuts, as well as the CMUP/CMX Trigger and Stub efficiencies [11] in Table 5.

Selection Criteria	Efficiency (%)
$\|z_0\| < 60$ cm	95.0 ± 0.4
All Track Cuts	93.6 ± 0.2
CMUP Trigger & All Stub Cuts	78.8 ± 1.1
CMX Trigger & All Stub Cuts	94.1 ± 0.7

Table 5: *Muon ID efficiencies.*

4.2 Calorimeter Ionization Cut Efficiency

Efficiencies were also calculated for the calorimetry highly ionizing cuts. We counted the number of cosmics with ionization values ($EMET$ and $HadET$) quadrupled that passed each cut. These cosmics represent the doubly-charged signal events and thus they were used in calculating the signal efficiencies seen in Table 6.

Variable(s) cut	Cut Value	# Signal events passing (out of 216,224)	Signal efficiency (%)
$EMET$	> 0.6 GeV	184,321	85.25 ± 0.08
$HadET$	> 4 GeV	191,790	88.70 ± 0.07
$EMET$ & $HadET$	> 0.6 GeV, > 4 GeV	175,333	81.09 ± 0.08

Table 6: *Calorimeter ionization cut efficiencies after cuts in Table 5 have been made.*

4.3 COTHW Ionization Cut Efficiency

Since there are limitations in measuring very small pulse widths recorded by $COTHW$, the lower tail of the quadrupled $COTHW$ variable is cut off. Therefore, it would be incorrect to quote any efficiency by simply counting the number of highly ionizing cosmic events that pass the 30ns cut. We chose to use the alternate method explained below for calculating the efficiency of this variable.

To begin, we needed to isolate a highly ionizing sample in the data that could not be part of the $H^{\pm\pm}$ signal. We used the Universal Curve predictions from [9] to draw theory curves of dE/dx vs. p_{track} for various particles, and then overlaid these curves on a scatter plot of data events. The data we use includes all positively charged tracks with ≥ 5 hits in ≥ 3 stereo superlayers and ≥ 3 axial superlayers. We also required $|d_0| \geq 1$ cm for these tracks in the data. The resulting graph can be seen in Figure 1. From this plot, we chose to isolate a proton band somewhere in the momentum range of 300-600 MeV which would have roughly the same $COTHW$ spectrum as our $Cosmic \times 4$ sample. We divided this momentum range into 50 MeV bins which can be seen in Figure 2. The rightmost peaks of the histogram correspond to a proton sample, and the curve with the highest dE/dx (300-350 MeV) is the one we will isolate for the efficiency calculation. Figure 3 shows this highly ionizing proton sample compared to our $COTHW \times 4$ cosmic sample. Although the proton sample is taken from a portion of the momentum curve that is slanted, our 50 MeV slice should be narrow enough to prevent any distortions or skewing of the shape. Since the proton sample does not have quite as large of $COTHW$ values, the efficiency we derive from this sample will be an underestimate of the true $H^{\pm\pm}$ efficiency.

In order to provide a cleaner sample of protons, we want to use the equal distribution of positive and negative pions and kaons to remove these additional peaks. Figure 4 shows the positively charged and negatively charged distributions overlaid. Subtracting these distributions gives us a much improved proton peak in Figure 5. We also show the $H^{\pm\pm}$ $COTHW$ distribution as predicted by the Universal Curve. It is clear from this theoretical prediction that the proton peak in the 300-350 MeV range is the correct one to use for measuring the efficiency of the $COTHW$ cut on $H^{\pm\pm}$ particles. Table 7 shows the $COTHW$ efficiency we found from the pion-subtracted distribution of protons in the 300-350 MeV momentum window. Since the only inefficiency is due to kaons near our proton peak and the $H^{\pm\pm}$ Universal Curve shows no efficiency loss, we believe our 35 ns cut on $COTHW$ is fully efficient. We apply a systematic of -0.5% to cover the alleged inefficiency from the low-momentum proton distribution.

Cut Value	# Proton events passing (out of 93,271)	Signal efficiency (%)
COTHW > 35 ns	92,865	99.56 ± 0.02

Table 7: *$COTHW$ cut efficiency after cuts in Table 5 have been made.*

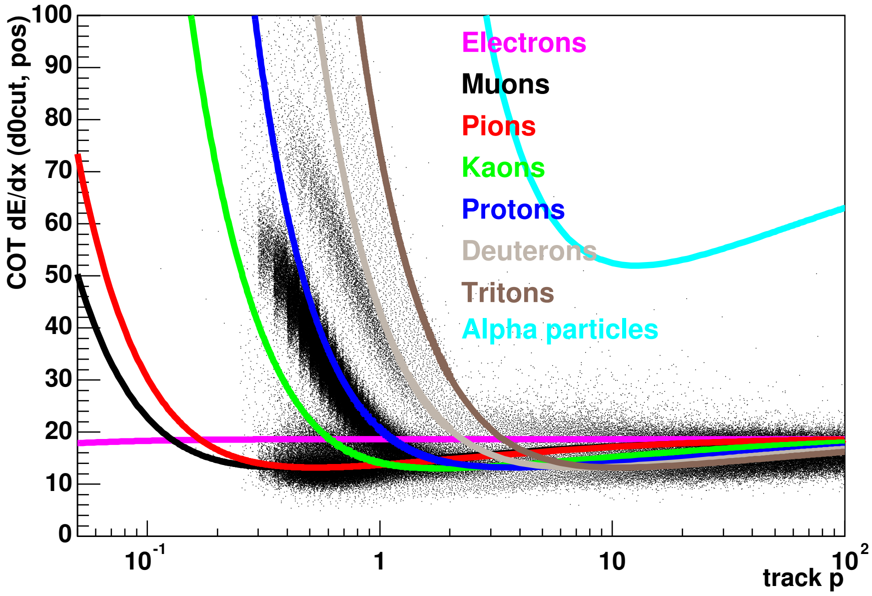

Figure 1: *Scatter plot of all positive tracks having ≥ 5 hits in ≥ 3 stereo SL's and ≥ 3 axial SL's, as well as $|d_0| \geq 1$ cm. The overlaid lines were calculated from the B group's Universal Curve prediction.*

4.4 Higgs ID Efficiency

The ID efficiency of a doubly-charged Higgs event is the product of the individual muon efficiency properly applied to two particles and the efficiencies of the high ionization cuts on $EMET$, $HadET$, and $COTHW$. Table 8 summarizes these efficiencies.

We address the issues involved in the use of muons for measuring the efficiency of a doubly charged particle. Muons may not give an accurate measurement due to edge effects

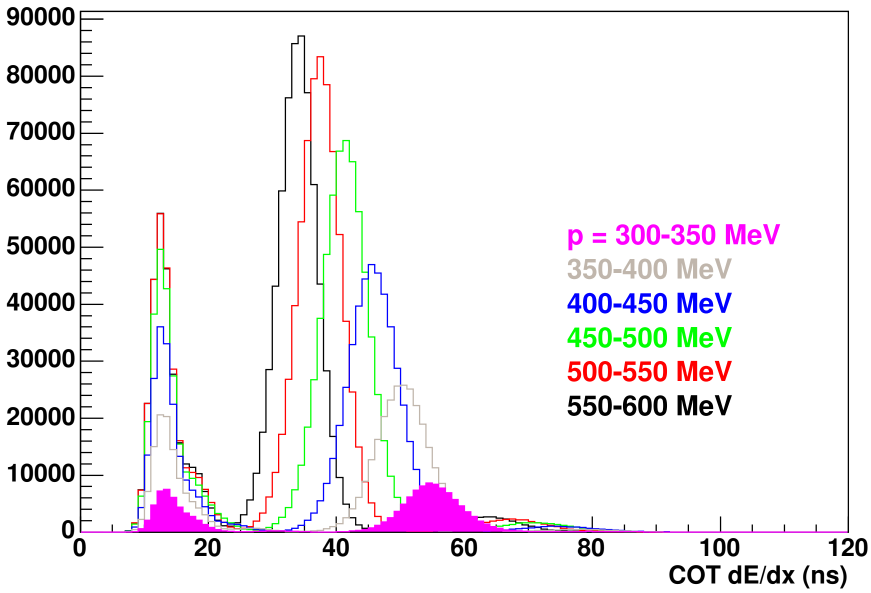

Figure 2: *Peaks on right correspond to a highly ionizing band of protons in 50 MeV bins of the scatter plot shown in Figure 1.*

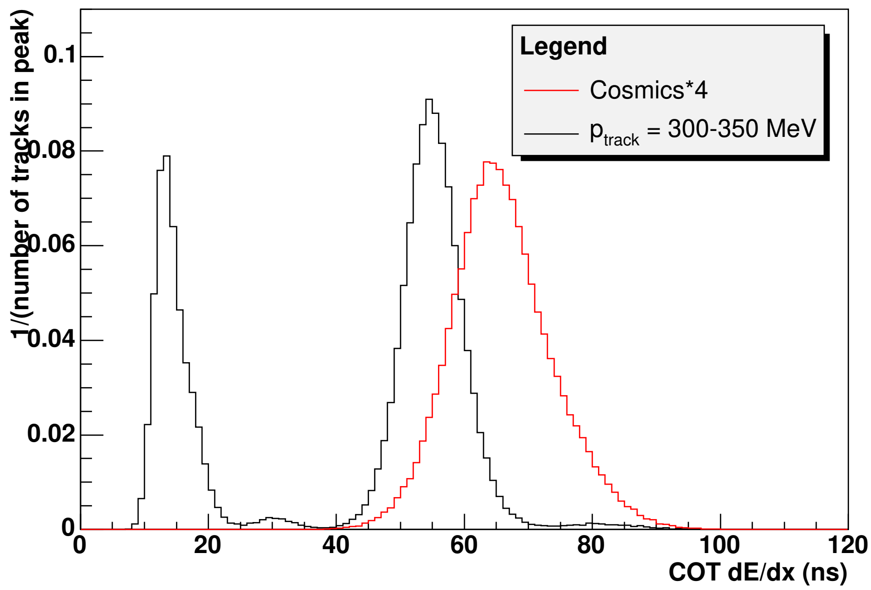

Figure 3: *Comparison of dE/dx values for highly ionizing proton sample and highly ionizing muon sample (Cosmic $\times$ 4). Since the peaks are not aligned, any efficiency calculated from the proton sample is to be taken as an underestimate of the true $COTHW$ efficiency for doubly-charged Higgs events.*

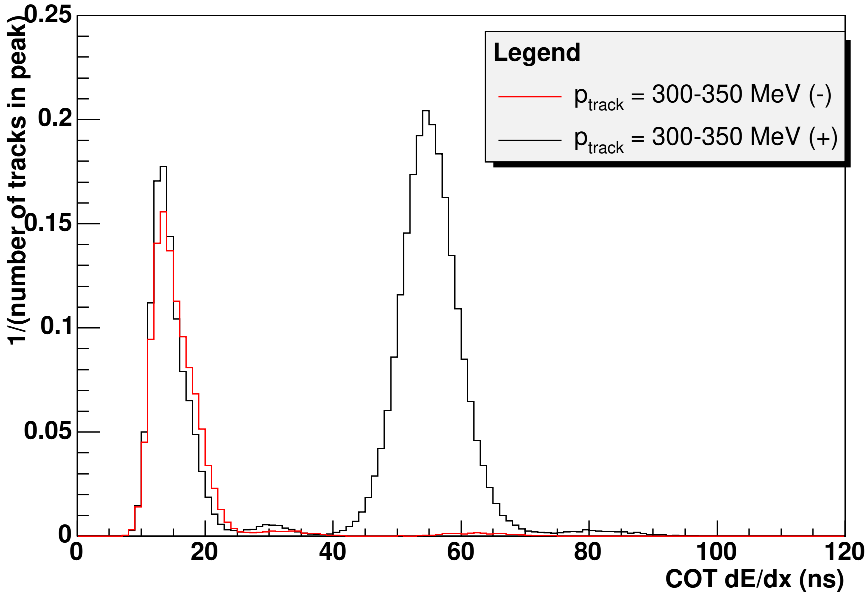

Figure 4: *Comparison of positively and negatively charged particles in the momentum window of 300-350 MeV. We will use the proton-antiproton assymetry to remove the pion and kaon contamination.*

in calorimeter towers, and due to differences in multiple scattering between muons and doubly-charged particles.

The edge effects would potentially affect our cut on the isolation ratio of the particle. To get an estimate of the edge effects involved, we estimated what percentage of the calorimeter tower's area is within 0.65 cm of the $z-$edge [1] of the tower. The width of this strip is estimated as follows. The 1σ error on the track extrapolation to the beamline in the z view is 0.35 cm, as determined from the distribution of the difference of z_0 of the two tracks in $Z \to \mu\mu$ decays (see Fig. 6). The beamline is 47 cm from the inner COT superlayer, compared to the extrapolation of 70 cm from the outer superlayer to the calorimeter. We therefore estimate the track error to be $0.35 \times 70/47 = 0.52$ cm at the calorimeter. We approximate the Gaussian error distribution of the track extrapolation by a uniform "box" distribution of equal area. A simple calculation shows that a box of width 1.25σ gives the same area (i.e. the same probability) as a unit-area Gaussian. This gives the estimate of 0.65 cm as the width of the strip along the $z-$edge of the tower in which the particle would actually have passed through the adjacent tower.

Each tower subtends an angle of 0.11 radians in η and 0.25 radians in ϕ, so if we estimate the calorimeter surface lies 2 meters from the interaction point, we compute a single tower

[1] The resolution in the $r-\phi$ view is $\approx 200\mu$m, as observed in the distribution of impact parameter of COT-only tracks. Since the $r-\phi$ resolution is negligible compared to the z-view resolution, we only consider the edge effect in the $z-$view.

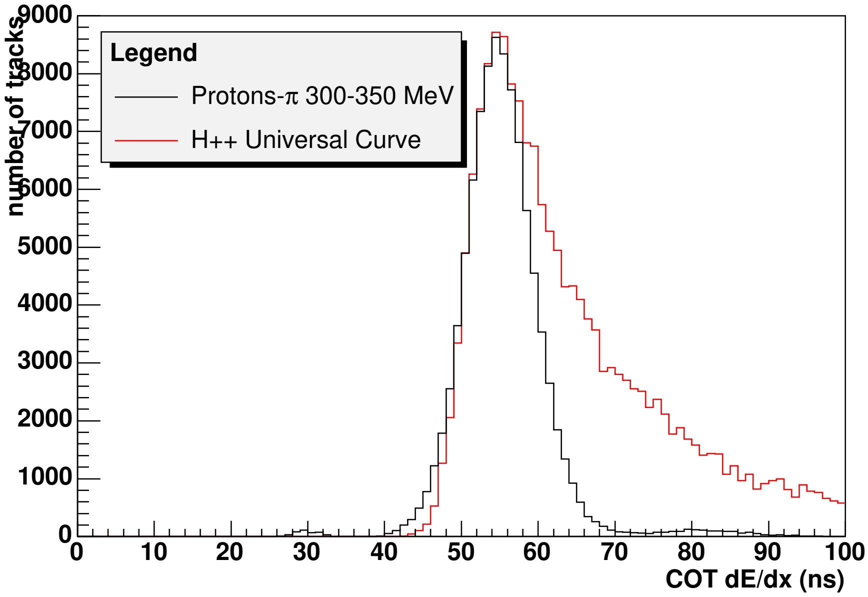

Figure 5: *The subtracted proton distribution (positively charged particles - negatively charged particles) used for measuring $H^{\pm\pm}$ efficiency. Some residual kaons produce the bump to the left of the primary peak. The peak of the distribution matches nicely with the $H^{\pm\pm}$ Universal Curve theoretical prediction.*

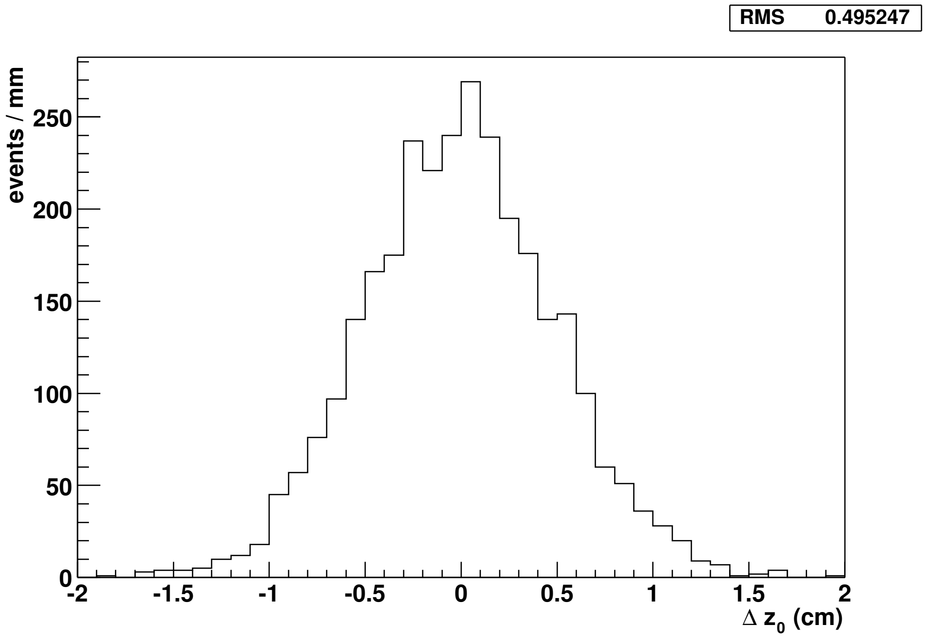

Figure 6: *The distribution of the difference of the z_0 of the two muon tracks in $Z \to \mu\mu$ decays. We obtain the z_0 resolution to be 0.35 cm based on $rms/\sqrt{2}$.*

surface area of about 1,100 cm^2. Considering only the area of this tower within 0.65 cm of the $z-$edge, we get 65 cm^2, which is 5.9% of the total area.

A doubly-charged Higgs as seen by the detector would have a mean p_T of about 50 GeV and would deposit on average roughly 9 GeV in the calorimeters (four times the average of a cosmic). Thus, the majority of the doubly-charged Higgs particles would fail the isolation ratio cut of 0.1 if their energy deposition were included in the isolation energy. To compute this fraction, we perform a "fast Monte Carlo" calculation based on the generator-level doubly-charged Higgs PYTHIA sample. For each doubly-charged Higgs particle, we sample the expected distributions of the calorimeter energy deposition (as measured from cosmic rays and scaled by a factor of 4) and compute the isolation ratio = (Calorimeter E_T) / (observed p_T). The denominator is obtained by dividing the generator-level p_T by 2. From the resulting histogram of the isolation ratio, we find the fraction passing the cut at 0.1. We find the fraction to vary from 20% at Higgs mass of 100 GeV to 38% at Higgs mass of 160 GeV. The increase is due to the p_T spectrum becoming harder as the Higgs mass increases. Since we are calculating a correction to a correction, we ignore the Higgs mass-dependence, and use the pass-fraction of 26% at Higgs mass [2] of 120 GeV. Thus, we estimate that 74% of the Higgs particles whose energy deposition is included in the isolation energy will fail the isolation cut.

As a result, the $H^{\pm\pm}$ candidates would fail the isolation ratio cut 5.9%×74% ≈ 4.4% of the time. To account for this potential effect causing the doubly-charged higgs to fail the isolation cut as it passes near an edge, we reduce the track efficiency from its "muon" value of $93.6 \pm 0.2\%$ to $89 \pm 4\%$, where the uncertainty is assigned conservatively to cover the magnitude of the edge effect.

Regarding the increased multiple scattering for doubly-charged particles, which could potentially affect the $|dx|$ cuts on the stub, this is investigated using muon tracks from Upsilon decays having $p_T \approx 10$ GeV, and no reduction in efficiency was observed [6]. The efficiency is decreased by $< 1\%$ for these low momentum particles. In this study, a change in p_T by a factor of three [3] makes no significant difference. The p_T of $H^{\pm\pm}$ bosons is larger than the p_T of $Z \rightarrow \mu\mu$ muons by a factor of 3, thus we expect negligible inefficiency due to multiple scattering.

Since both particles come from the same vertex, the $|z_0|$ efficiency can stand as it is, but the Track Cuts are required of each particle separately, so we must square this efficiency to find the net Z efficiency. The same applies for all of the high ionization cuts, since each particle must pass the cut. These efficiencies are summarized in Table 8. The Trigger and Stub Cuts are only required for at least one of the two particles, therefore we need to calculate these efficiencies using the binomial formula:

$$\begin{aligned} \text{P(at least one)} &= 1 - \text{P(neither)} \\ &= 1 - (1-\epsilon_1)(1-\epsilon_2) \end{aligned} \tag{3}$$

[2]Our Higgs mass sensitivity extends to ≈110 GeV for right-handed couplings and ≈130 GeV for left-handed couplings

[3]the mean p_T of muons from Z decays is ≈ 35 GeV

where ϵ_1 and ϵ_2 are the Trigger and Stub efficiencies corresponding to the muon detectors being considered. For example, if both of the particles pass through the CMUP, then the efficiency for at least one of them triggering and leaving a stub would be found by using the CMUP Trigger and Stub efficiency for both ϵ_1 and ϵ_2 in Equation 3. The three possible categories (CMUP×2, CMX×2, and CMUP/CMX) for this efficiency have been calculated and can be found in Table 9, along with the fraction of $H^{\pm\pm}$ MC measured for each category.

Selection Criteria	Loose Efficiency (%)	Tight Efficiency (%)
$\lvert z_0 \rvert < 60$ cm	95.0 ± 0.4	95.0 ± 0.4
All Track Cuts	79.2 ± 8.0	79.2 ± 8.0
EMET & HadET Cuts	-	65.76 ± 0.09
COTHW cut	$100.0^{+0.0}_{-1.0}$	$100.0^{+0.0}_{-1.0}$
All above	75.2 ± 7.6	49.5 ± 5.0

Table 8: *$H^{\pm\pm}$ ID efficiencies except for CMUP/CMX Trigger and Stub efficiencies which are dependent on the Higgs mass and can be found in Table 9.*

$H^{\pm\pm}$ mass	CMUP×2 Eff.	CMUP×2 fraction	CMX×2 Eff.	CMX×2 fraction
90 GeV	0.955 ± 0.003	0.582 ± 0.005	0.997 ± 0.001	0.066 ± 0.002
100 GeV	0.955 ± 0.003	0.574 ± 0.005	0.997 ± 0.001	0.070 ± 0.002
130 GeV	0.955 ± 0.003	0.593 ± 0.004	0.997 ± 0.001	0.064 ± 0.002
160 GeV	0.955 ± 0.003	0.603 ± 0.004	0.997 ± 0.001	0.063 ± 0.002

$H^{\pm\pm}$ mass	CMUP/CMX Eff.	CMUP/CMX fraction	Net Trigger Eff.
90 GeV	0.987 ± 0.002	0.352 ± 0.004	0.969 ± 0.007
100 GeV	0.987 ± 0.002	0.355 ± 0.004	0.968 ± 0.007
130 GeV	0.987 ± 0.002	0.342 ± 0.004	0.968 ± 0.006
160 GeV	0.987 ± 0.002	0.334 ± 0.004	0.968 ± 0.006

Table 9: *CMUP and CMX Trigger and Stub efficiencies with their fraction of occurence in the $H^{\pm\pm}$ Monte-Carlo having masses of 90, 100, 130, and 160 GeV.*

$H^{\pm\pm}$ mass	Net Loose $H^{\pm\pm}$ Efficiency	Net Tight $H^{\pm\pm}$ Efficiency
90 GeV	0.729 ± 0.092	0.480 ± 0.061
100 GeV	0.728 ± 0.092	0.479 ± 0.061
130 GeV	0.728 ± 0.092	0.479 ± 0.061
160 GeV	0.728 ± 0.092	0.479 ± 0.061

Table 10: *Net $H^{\pm\pm}$ ID efficiencies using either loose or tight ionization cuts. These were calculated from the efficiencies listed in Tables 8 and 9.*

5 Fake Rates

5.1 Measuring Muon $\to H^{\pm\pm}$ Fake Rates

We select cosmic rays from CDF Run II data (sample defined in Section 1.1) as a pure muon sample for this fake rate measurement. The cosmics were tagged using tightened selection cuts from the COT cosmic-ray tagger [10]. We select cuts on our three dE/dx variables to identify high ionization tracks. The respective fake rates for the cuts are then measured by observing how many cosmics in the sample pass these high ionization cuts.

We also include a representation of a high ionization sample in our figures by multiplying the dE/dx quantity for each cosmic by a factor of four and plotting that histogram together with the original cosmic histogram. This gives a description of how the signal for a doubly-charged particle should look. Figure 7 gives these histograms for $EMET$ along with the cut value chosen, while Figures 8 and 9 show the same for $HadET$ and $COTHW$ respectively. The high ionization cuts are listed in Table 3. The $H^{\pm\pm}$ selection includes the track and stub cuts in Table 1 and these high ionization cuts in Table 3.

Fake rates were calculated by counting the number of cosmic events passing (above) the respective cut values. Fake rates were also found for combined variables, and these rates confirm that our three variables are not highly correlated. All the relevant fake rates are shown in Table 11.

Efficiencies were also calculated for these high ionization cuts and are given in Section 4.

In order to find an upper limit for the fake rate on the combined ionization cuts, we lowered the cut value of $COTHW$ to 20 ns. Using this cut value, we found the combined fake rate of all three variables to be $(0.01619 \pm 0.00274)\%$ which is estimated to be high by a factor of roughly 10,000 (since there were 10,566 fakes for the $COTHW$ variable alone when cut at 20 ns and on the order of 1 fake when cut at 35 ns). Thus, the fake rate of the combined variables with all high ionization cuts listed in Table 3 is estimated to be:

$$\begin{aligned} \text{Net } \mu \to H^{\pm\pm} \text{ fake rate} &= f_1 \times f_2 \\ &= (1.5 \pm 1.5) \times 10^{-8}, \end{aligned} \tag{4}$$

where f_1 is the fake rate given in the sixth line of Table 11 and f_2 is from the eighth line

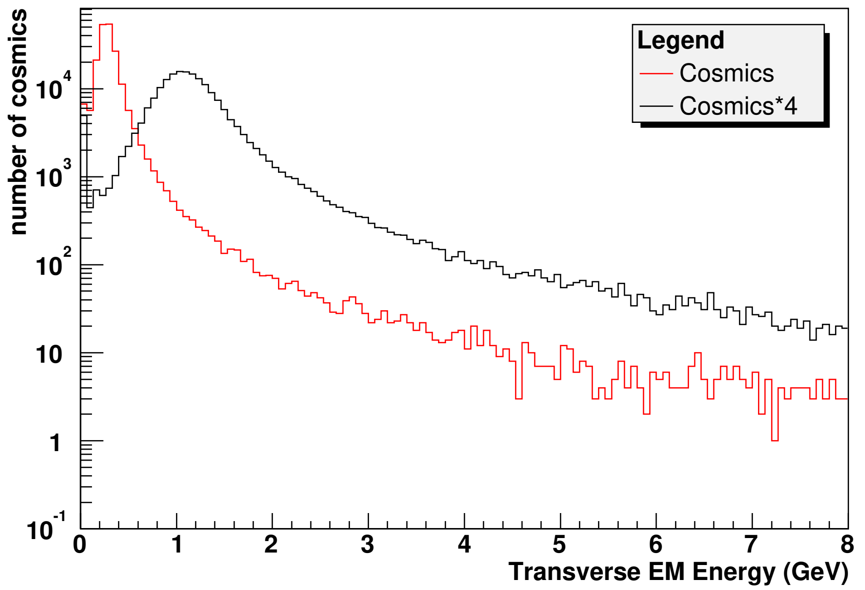

Figure 7: *Out of 216,224 cosmic events, 11,612 passed the 0.6 GeV cut on EMET. This gives a fake rate for this variable alone of* $(5.37 \pm 0.05)\%$*. Of the "Cosmics × 4" events 184,321 passed the same cut, giving a signal efficiency of* $(85.25 \pm 0.08)\%$*.*

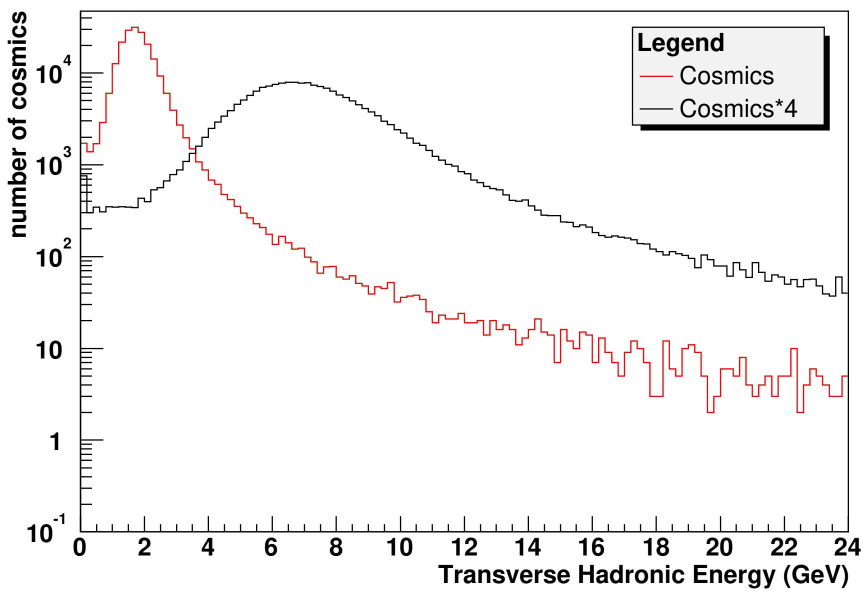

Figure 8: *Out of the same 216,224 cosmics, only 6,486 passed the 4 GeV cut on HadET. Thus, the fake rate for this variable was found to be* $(3.00 \pm 0.04)\%$*. Of the highly ionizing "Cosmics × 4" events, 191,790 passed the cut, giving a signal efficiency of* $(88.70 \pm 0.07)\%$*.*

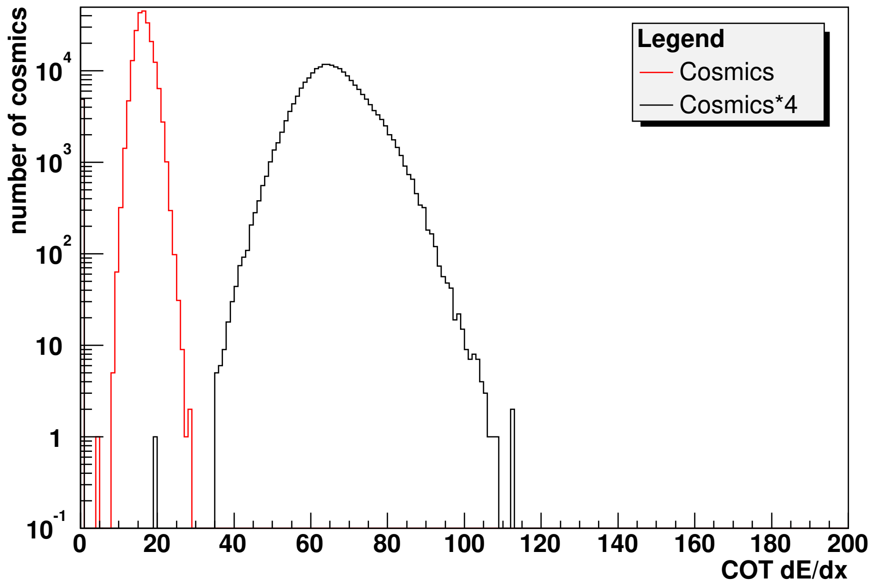

Figure 9: *None of the 216,224 cosmics passed the 35 ns COTHW cut, therefore the individual fake rate for this variable is 0.00%. The experimental limits of recording very small pulse widths do not permit us to use this sample for measuring COTHW cut efficiency.*

of the same table. f_2 is not calculated from the entire cosmics sample, but only from those events passing the 20 ns *COTHW* cut. Their product is the bottom line of that table and is the same as that in Equation 4 above. Thus it is apparent that the fake rate due to highly ionizing muons is quite small.

5.2 Muon $\rightarrow H^{\pm\pm}$ Fake Rate Systematics

To further understand high ionization for muons passing through the COT, we did a systematics study of the *COTHW* variable. For this study we lowered the *COTHW* cut to 20 ns in order to introduce some cosmics having higher ionization so a fake rate could be calculated. Then we plotted this modified fake rate as a function of three variables.

The first relationship we analyzed was that between fake rate and COT track multiplicity. This quantity is defined as the number of tracks with at least one hit in the COT. Figure 10 illustrates the rise in the fake rate as a direct result of more tracks in the COT. This is possibly due to the merging of nearby hits thus artificially increasing the pulse-width. Figure 11 shows that the Z and W events are much more track-rich than the cosmic events which we used to calculate the fake rate, therefore we need to scale our fake rate to a higher value. To do this, we found the mean of the track multiplicity for both the W and Z event candidates to be roughly 30 tracks. The appropriate *COTHW* fake rate to use for this increased number of tracks in the COT was taken from Figure 10 to be $7.00 \pm 0.07\%$. The error on this rate

Variable(s) cut	Cut value	# Passing	Tight μ Fake rate (%)
Cosmic Tagger		216,224	
EMET	> 0.6 GeV	11,612	5.37 ± 0.05
HadET	> 4 GeV	6,486	3.00 ± 0.04
EMET & HadET	> 0.6 GeV, > 4 GeV	763	0.353 ± 0.013
COTHW	> 20 ns	10,566	4.89 ± 0.05
EMET, HadET, & COTHW	> 0.6 & 4 GeV, > 20 ns	35	0.01619 ± 0.00274
COTHW	> 20 ns	10,566	
COTHW	> 35 ns	0 (1 ± 1)	0.00946 ± 0.00946
Tight Ionization	from Table 3	0	$(1.5 \pm 1.5) \times 10^{-6}$

Table 11: *Muon $\rightarrow H^{\pm\pm}$ fake rates with tight ionization cuts.*

Variable(s) cut	Cut value	# Passing	Loose μ Fake rate (%)
Cosmic Tagger		216,224	
COTHW	> 35 ns	0 (1 ± 1)	$(4.6 \pm 4.6) \times 10^{-4}$
Loose Ionization	from Table 3	0	$(4.6 \pm 4.6) \times 10^{-4}$

Table 12: *Muon $\rightarrow H^{\pm\pm}$ fake rates with loose ionization cuts.*

was found by scaling the error on the fake rate for $COTHW$ (20 ns cut) found using cosmic events (0.05%) by the ratio of the new fake rate (7.00%) to the old (4.89%). The net fake rate using all the high ionization cuts in Table 3 also must be scaled by this ratio, giving us new $\mu \to H^{\pm\pm}$ fake rates of $(2.1 \pm 2.1)\% \times 10^{-6}$ for the tight search and $(6.6 \pm 6.6)\% \times 10^{-4}$ for the loose.

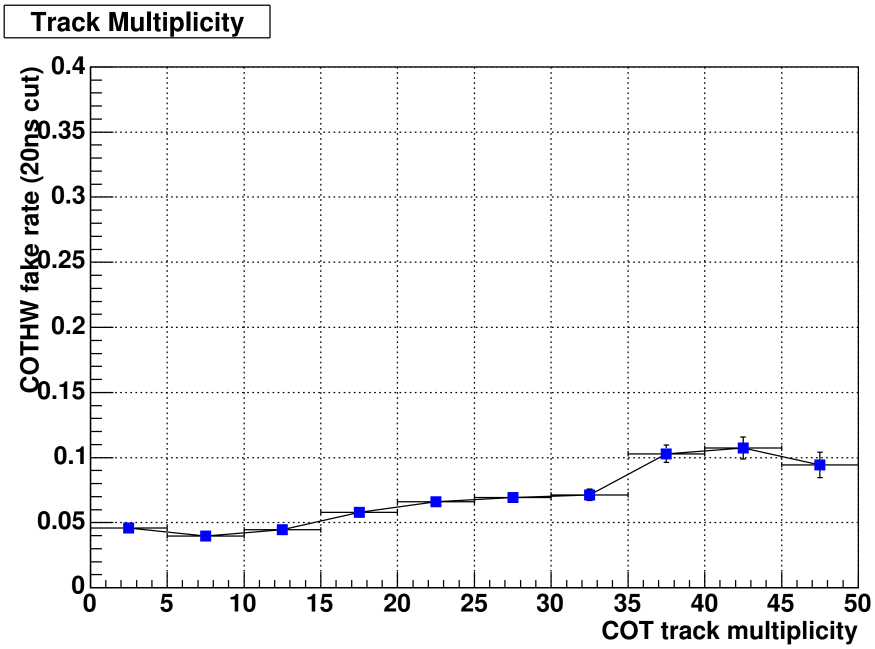

Figure 10: *Systematic of $COTHW$ showing the clear increase in fake rate as more tracks populate the COT.*

Upon the suggestion of others, we also examined COT track density in the 0.4 cone surrounding the muon. These tracks are more likely to directly effect the ionization in the COT by artificially widening the muon's pulse width. Only tracks having at least one COT hit are counted, and we include the primary track in this value. We show the corresponding fake rate distribution for cosmics by the number of tracks found in the cone in Figure 12. The number of tracks in this cone for Z, W, and cosmic events can be seen in Figure 13. Again, the fake rates increase as the number of tracks in the cone increases, prompting us to scale our cosmic sample fake rate up for collider events. We find the mean number of tracks in the cone for W and Z events to be 1.85 tracks (with only 1.14 tracks on average in cosmic events). We take the $COTHW$ fake rate for 2 tracks in the cone (from Figure 12) of $5.92 \pm 0.19\%$. Scaling up our final $\mu \to H^{\pm\pm}$ fake rate by the ratio between this new fake rate and the old $COTHW$ fake rate of $4.89 \pm 0.05\%$ results in a scaled fake rate of $(1.8 \pm 1.8(stat) \pm 0.3(syst))\% \times 10^{-6}$ for the tight search and $(5.6 \pm 5.6(stat) \pm 1.0(syst))\% \times 10^{-4}$ for the loose. We use these fake rates in place of the ones scaled by track multiplicity above, and give systematic errors based on the difference between the two methods of scaling for track density.

Similarly, isolation fraction measures how much energy is deposited in a window surround-

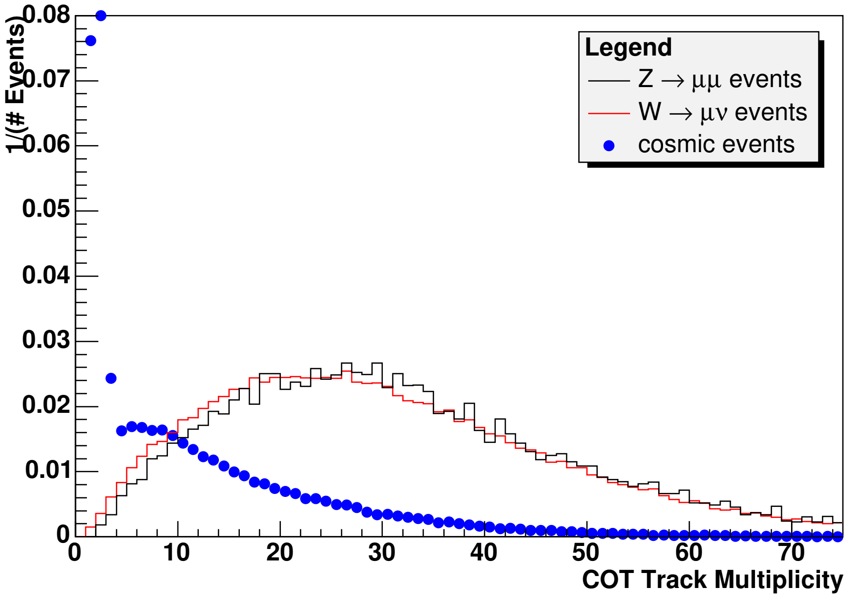

Figure 11: *Comparison of relative COT track multiplicities for Z events, W events, and cosmic events. The mean track multiplicities for Z and W events were found to be 30.8 and 29.6 respectively.*

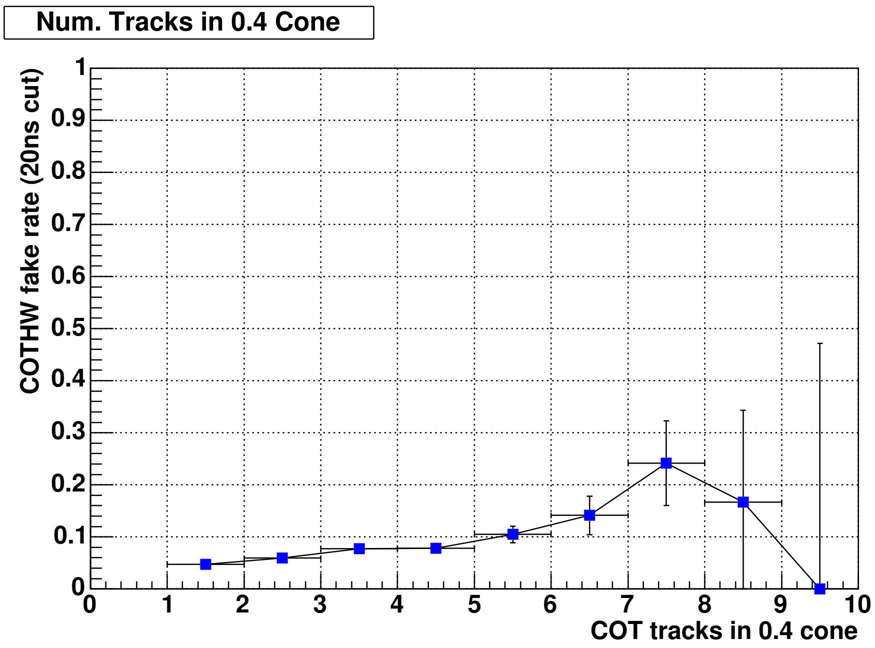

Figure 12: *Systematic of COTHW showing the clear increase in fake rate as more tracks surround the muon track.*

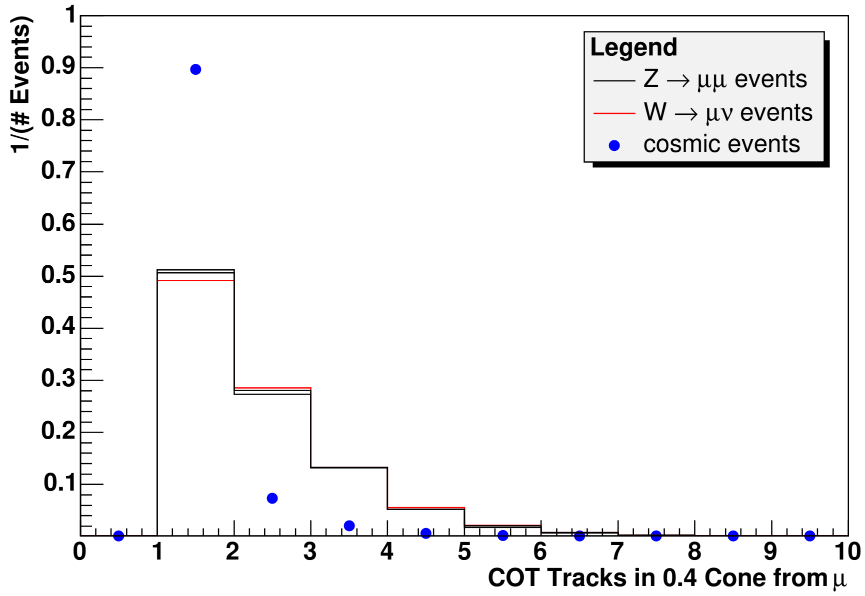

Figure 13: *Comparison of relative number of COT tracks in 0.4 cone for Z events, W events, and cosmic events. The mean number of tracks in the cone for Z and W events were found to be 1.83 and 1.88 respectively, with only 1.14 tracks in the cone on average for cosmic events.*

ing the track in question and is also a good quantity for this systematics study. Figure 14 shows the fake rate measured by $COTHW$ as a function of the isolation fraction. It appears from this figure that the fake rate is not highly correlated to this variable.

The final systematic comparison studies the fake rate as a function of the total energy deposited by the muon in the hadronic and electromagnetic calorimeters. Since this is a calorimetric quantity, we expect it to be relatively flat if the $COTHW$ fake rate is not highly correlated to the calorimetric dE/dx quantities and Figure 15 confirms this.

5.3 Measuring Electron → $H^{\pm\pm}$ Fake Rates

We use $W \to e\nu$ Monte-Carlo events ($\sim$ 1,150,000 events from the `wtop0e` dataset) as an electron sample for this fake rate measurement. We look in this electron sample for reconstructed "muons" passing the Track Cuts from Table 1. Upon making the Track Cuts we calculated the fake rate by counting the fraction which also pass the Stub Cuts in Table 1 and the three high ionization cuts in Table 3.

The $COTHW$ variable was not properly simulated in electron MC as can be seen in Figure 16, so we shifted the $COTHW$ variable in the MC by ~ -10 and smeared it with both a random gaussian and an exponential function to make it look like the electron data. The scaled electron MC $COTHW$ can be seen in Figures 17.

Table 13 shows the $e \to H^{\pm\pm}$ fake rates we found for both individual and combined

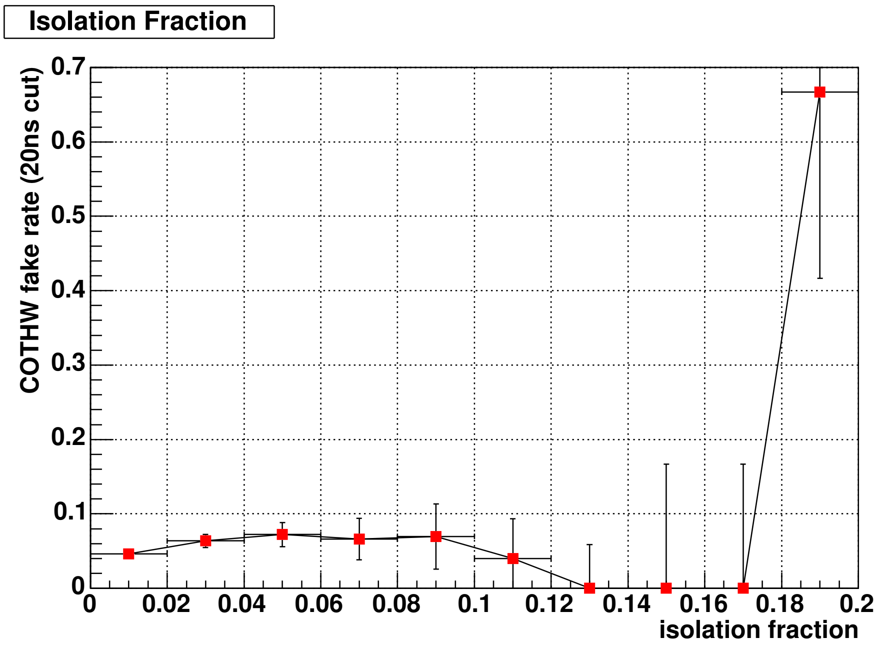

Figure 14: *Another systematic of COTHW showing a slight upward trend in the fake rate as the region near the track becomes less isolated.*

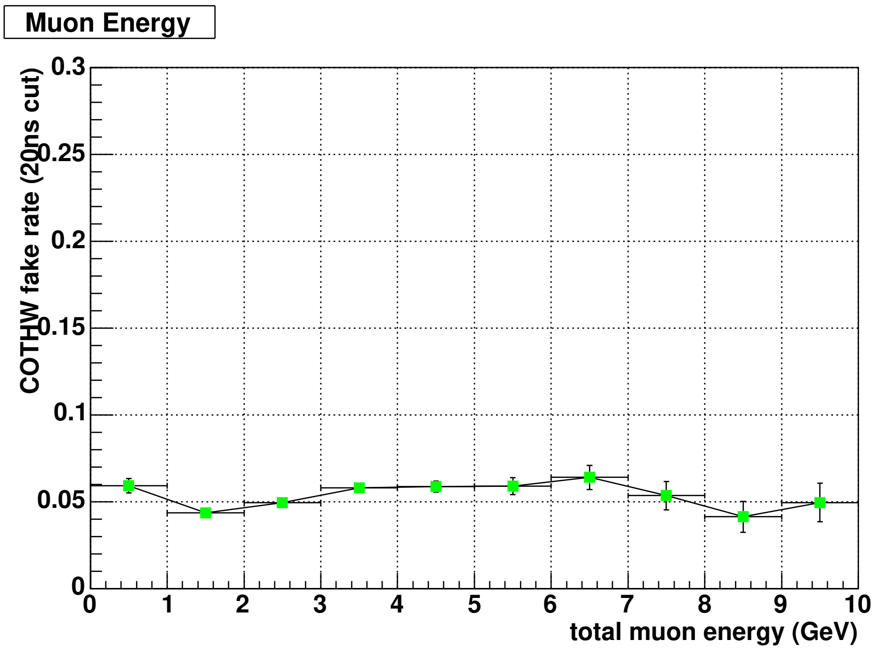

Figure 15: *Final COTHW systematic plot showing the uncorrelated nature of the tracking dE/dx quantity to the ionization quantities measured by the calorimeter.*

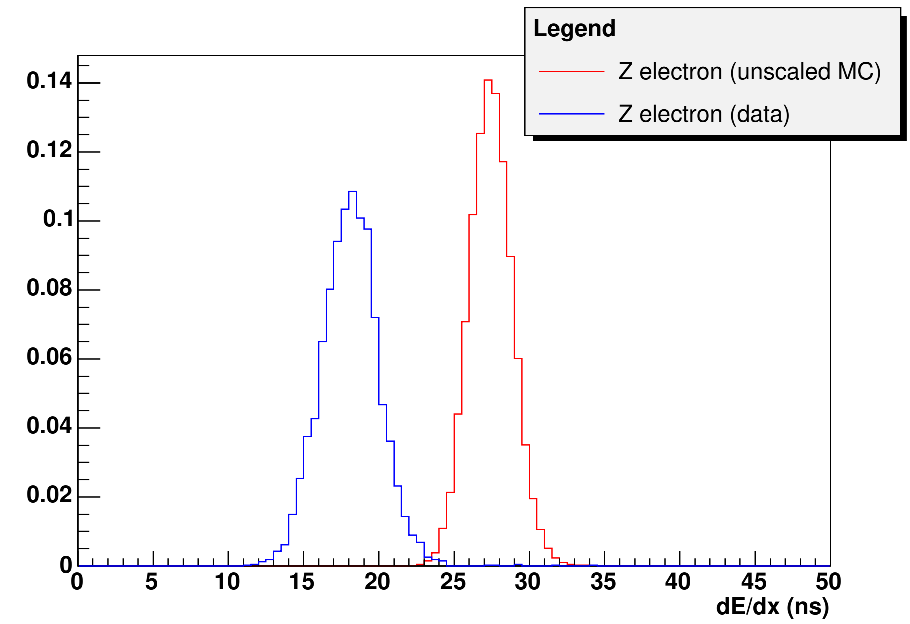

Figure 16: *The electron Monte-Carlo events clearly have too large of values for COTHW and must be shifted.*

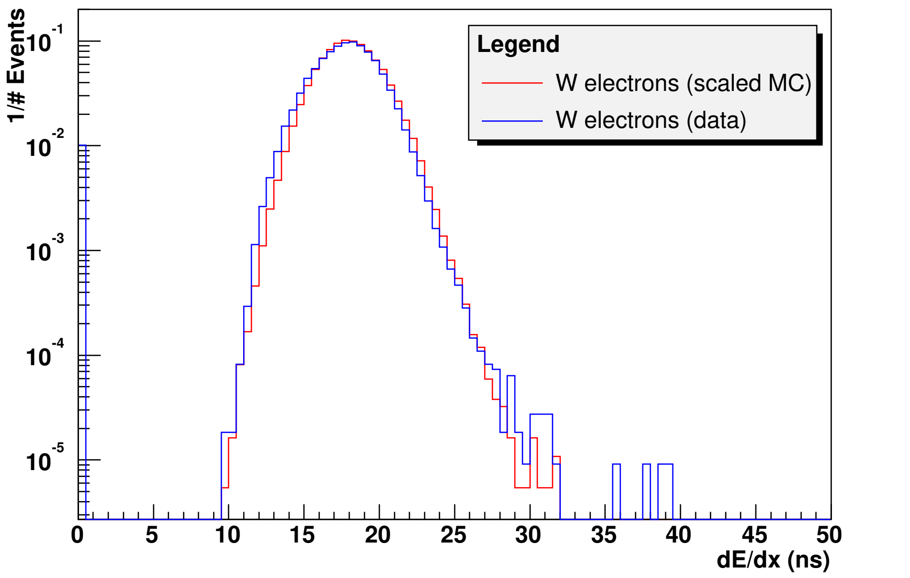

Figure 17: *After shifting the MC by* ~ -10 *and smearing with gaussian and exponential random numbers, there is much better agreement with the electron data.*

ionization variables. Similar to Equation 4 in the $\mu \rightarrow H^{\pm\pm}$ fake rate study, the fake rate of the high ionization cuts listed in Table 3 and the Stub Cuts in Table 1 needed to be factorized for electrons since no events passed all these cuts:

$$\begin{aligned} \text{Net } e \rightarrow H^{\pm\pm} \text{ fake rate} &= f_3 \times f_4 \times f_5 \\ &= (2 \pm 2) \times 10^{-10}, \end{aligned} \tag{5}$$

where the factor f_3 comes from the sixth line, f_4 from the eighth, and f_5 from the tenth line in Table 13. The bottom line $e \rightarrow H^{\pm\pm}$ fake rate is in the last line of that table and comes from the product of these three factors as shown in Equation 5 above.

Variable(s) cut	Cut value	# Passing	Tight e Track Fake rate (%)
Track	from Table 1	272,734	
EMET	> 0.6 GeV	264,570	97.01 ± 0.03
HadET	> 4 GeV	6,025	2.21 ± 0.03
EMET & HadET	> 0.6 GeV, > 4 GeV	3,352	1.23 ± 0.02
COTHW	> 20 ns	44,500	16.32 ± 0.07
EMET, HadET, & COTHW	> 0.6 & 4 GeV, > 20 ns	556	0.204 ± 0.009
COTHW	> 20 ns	44,500	
COTHW	> 35 ns	0 (1 ± 1)	0.0022 ± 0.0022
Tight Ionization	from Tables 1 & 3	0	$(4.5 \pm 4.5) \times 10^{-6}$

Variable(s) cut	Cut value	# Passing	Tight e Muon Fake rate (%)
Track	from Table 1	272,734	
EMET	> 0.6 GeV	264,570	97.01 ± 0.03
HadET	> 4 GeV	6,025	2.21 ± 0.03
EMET & HadET	> 0.6 GeV, > 4 GeV	3,352	1.23 ± 0.02
COTHW	> 20 ns	44,500	16.32 ± 0.07
EMET, HadET, & COTHW	> 0.6 & 4 GeV, > 20 ns	556	0.204 ± 0.009
EMET & HadET	> 0.6 GeV, > 4 GeV	3,352	
Stub	from Table 1	1	0.030 ± 0.030
COTHW	> 20 ns	44,500	
COTHW	> 35 ns	0 (1 ± 1)	0.0022 ± 0.0022
Stub & Tight Ion.	from Tables 1 & 3	0	$(1.4 \pm 1.4) \times 10^{-9}$

Table 13: *Electron* $\rightarrow H^{\pm\pm}$ *fake rates with tight ionization cuts.*

Variable(s) cut	Cut value	# Passing	Loose e Track Fake rate (%)
Track	from Table 1	272,734	
COTHW	> 35 ns	0 (1 ± 1)	0.00037 ± 0.00037
Loose Ionization	from Tables 1 & 3	0	$(3.7 \pm 3.7) \times 10^{-4}$

Variable(s) cut	Cut value	# Passing	Loose e Muon Fake rate (%)
Track	from Table 1	272,734	
Stub	from Table 1	1	$(3.7 \pm 3.7) \times 10^{-4}$
COTHW	> 20 ns	44,500	
COTHW	> 35 ns	0 (1 ± 1)	0.0022 ± 0.0022
Stub & Loose Ion.	from Tables 1 & 3	0	$(8.2 \pm 8.2) \times 10^{-9}$

Table 14: *Electron* $\rightarrow H^{\pm\pm}$ *fake rates with loose ionization cuts.*

5.4 Measuring $\tau \rightarrow H^{\pm\pm}$ Fake Rates

For the measurement of taus faking doubly charged Higgs, we look at a MC sample of 1 million taus from W in the `wewk4t` dataset. Since muon and electron final products are included in our previous two fake rates, we want this fake rate to include only taus decaying hadronically. We select these hadronic decays by requiring a jet having $E_T > 25$ GeV and $\eta < 1.0$. Only tracks that are reconstructed within $\Delta R < 0.7$ of this primary jet are used, where $\Delta R = \sqrt{\Delta\eta^2 + \Delta\phi^2}$.

We provide two different fake rates from our tau sample. The first is for a hadronic tau faking a highly ionizing track, thus passing all the Track Cuts in Table 1 and the three highly ionizing cuts in Table 3. The second fake rate is for hadronic taus faking a highly ionizing muon, therefore it must pass the Stub Cuts in Table 1 in addition to the cuts made in calculating the previous fake rate. Since no events pass both the Stub Cuts and the high ionization cuts, we factorize this fake rate by requiring these two cut categories separately. Both fake rates are derived in Table 15. Since we know from the electron MC that the $COTHW$ variable is not properly modeled in the simulation, we apply the same scaling and smearing corrections to the variable in the tau sample as we show in Figure 17.

5.5 Measuring QCD $\rightarrow H^{\pm\pm}$ Fake Rates

Our sample of unbiased jets is obtained from QCD data triggered on the `Jet_100` triggers. This mean p_T of this sample is approximately the same as the mean p_T for the stable $H^{\pm\pm}$. We make the assumption that the maximum E_T jet is the one responsible for firing the jet trigger. We have compared fake rates for tracks having $\Delta R > 0.7$ of the primary jet to those inside that cone, where $\Delta R = \sqrt{\Delta\eta^2 + \Delta\phi^2}$. We combine the two samples for calculating

Variable(s) cut	Cut value	# Passing	Tight Tau Track fake rate (%)
Hadronic Taus	jet $E_T > 25$, $\eta < 1.0$	61,084	
Track & Tight Ionization	from Tables 1 & 3	0 (1 ± 1)	0.0016 ± 0.0016

Variable(s) cut	Cut value	# Passing	Tight Tau Muon fake rate (%)
Hadronic Taus	jet $E_T > 25$, $\eta < 1.0$	61,084	
Track & Tight Ionization	from Tables 1 & 3	0 (1 ± 1)	0.0016 ± 0.0016
Track	from Table 1	4,050	
Track & Stub	from Table 1	5	0.123 ± 0.055
Track, Stub, and Tight Ion.	from Tables 1 & 3	0	$(2.0 \pm 2.0) \times 10^{-6}$

Table 15: $\tau \to H^{\pm\pm}$ *Track and Muon fake rates with tight ionization cuts.*

Variable(s) cut	Cut value	# Passing	Loose Tau Track fake rate (%)
Hadronic Taus	jet $E_T > 25$, $\eta < 1.0$	61,084	
Track & Loose Ionization	from Tables 1 & 3	0 (1 ± 1)	0.0016 ± 0.0016

Variable(s) cut	Cut value	# Passing	Loose Tau Muon fake rate (%)
Hadronic Taus	jet $E_T > 25$, $\eta < 1.0$	61,084	
Track & Loose Ionization	from Tables 1 & 3	0 (1 ± 1)	0.0016 ± 0.0016
Track	from Table 1	4,050	
Track & Stub	from Table 1	5	0.123 ± 0.055
Track, Stub, and Loose Ion.	from Tables 1 & 3	0	$(2.0 \pm 2.0) \times 10^{-6}$

Table 16: $\tau \to H^{\pm\pm}$ *Track and Muon fake rates with loose ionization cuts.*

our fake rates and provide systematic errors to cover the differences we find in the fake rates when calculating inside-jet and outside-jet separately.

We select a base track sample that pass the cuts in Table 17. We then check for highly-ionizing events in this sample by counting the number of tracks which pass both the Track Cuts in Table 1 and the highly ionizing cuts in Table 3. We perform a similar process to find the QCD *Muon* fake rate by counting the number of tracks in the jet samples which pass our base muon cuts in Table 17 and the number passing the $H^{\pm\pm}$ ID cuts in Table 3. These fake rates and the numbers used to find them are all found in Table 19.

We also looked for a p_T dependence in our track fake rate using loose ionization cuts. This was the only sample with high enough statistics for a potentially meaningful result. Table 18 shows the fake rates for tracks having p_T greater than or less than 40 GeV (the mean of the momentum distribution), as well as for tracks inside or outside the primary jet (an inside jet track is defined as having $\Delta R < 0.7$ from the highest E_T jet in the event). The high p_T tracks have a larger fake rate for those tracks both inside and outside the leading jet. Since the mean of the $H^{\pm\pm}$ p_T distribution is in the 40 GeV range, we apply no p_T dependent fake rates. We show systematic errors which cover the differences in fake rates for particles whose p_T lies above 40 GeV or whose p_T lies below 40 GeV.

Variable	Cut
Base Track	
ΔR from primary jet	> 0.7
$\|z_0\|$	< 60.0 cm
# Stereo hits	≥ 3 SL with ≥ 5 hits or COT layer < 96
# Axial hits	≥ 3 SL with ≥ 5 hits or COT layer < 96
$\|d_0\|$	< 0.2 cm
(isolation in R=0.4 cone)/p_T	< 1.0
p_T	> 20 GeV
ρ_{COT}	> 140 cm
Cosmic Ray Veto	
Base Muon	
All Base Track cuts	(see above)
$\|\Delta x_{CMU}\|$	< 3.0 cm
$\|\Delta x_{CMP}\|$	< 5.0 cm
$\|\Delta x_{CMX}\|$	< 6.0 cm

Table 17: *Base Track and Base Muon Cuts used in calculating the QCD fake rates.*

A confirmation of the overestimate of the QCD Muon fake rate using jet data came through the analysis of a control sample within the muon data. We currently wish to

Track selection	# Tracks passing Loose ionization cuts	# of Base tracks	Fake rate (%)
$p_T < 40$ GeV Inside jet	6	188,172	0.00319 ± 0.00130
$p_T < 40$ GeV Outside jet	85	159,401	0.0533 ± 0.0058
$p_T > 40$ GeV Inside jet	31	191,606	0.0162 ± 0.0029
$p_T > 40$ GeV Outside jet	82	100,151	0.0819 ± 0.0090

Table 18: *Loose QCD Track $\rightarrow H^{\pm\pm}$ fake rates in bins of inside/outside jet and high/low p_T.*

Variable(s) cut	Cut value	# Passing	Tight QCD Track fake rate (%)
Base Track	from Table 17	639,330	
Track & Tight Ion.	from Tables 1 & 3	18	$0.00282 \pm 0.00066(stat)^{+0.00034}_{-0.00051}(syst)$

Variable(s) cut	Cut value	# Passing	Tight QCD Muon fake rate (%)
Base Muon	from Table 17	5,416	
Track & Stub	from Table 1	354	6.54 ± 0.34
+ EMET	> 0.6 GeV	94	1.74 ± 0.18
+ HadET	> 4 GeV	69	1.27 ± 0.15
+ EMET, HadET	> 0.6 GeV, > 4 GeV	46	0.849 ± 0.125
+ EMET, HadET, COTHW	> 0.6, 4 GeV, > 20 ns	12	0.222 ± 0.064
+ COTHW	> 35 ns	1	1.82 ± 1.80
Track, Stub, & Tight Ion.	from Tables 1 & 3	1	0.0185 ± 0.0185

Table 19: *$QCD \rightarrow H^{\pm\pm}$ Track and Muon fake rates with tight ionization cuts. The Track fake rate includes systematic errors to cover the range between the fake rates for samples both inside and outside the primary jet. The statistics are too low to include systematic errors for p_T dependence as well.*

Variable(s) cut	Cut value	# Passing	Loose QCD Track fake rate (%)
Base Track	from Table 17	639,330	
Track & Loose Ion.	from Tables 1 & 3	204	$0.0319 \pm 0.0022(stat)^{+0.0500}_{-0.0287}(syst)$

Variable(s) cut	Cut value	# Passing	Loose QCD Muon fake rate (%)
Base Muon	from Table 17	5,416	
Track & Stub	from Table 1	354	6.54 ± 0.34
+ COTHW	> 35 ns	1	0.0185 ± 0.0185
Track, Stub, & Loose Ion.	from Tables 1 & 3	1	0.0185 ± 0.0185

Table 20: *$QCD \to H^{\pm\pm}$ Track and Muon fake rates with loose ionization cuts. The Track fake rate includes systematic errors to cover the range between the fake rates for $p_T > 40$ GeV and $p_T < 40$ GeV samples for both inside and outside the primary jet.*

preserve the blind status of the topology containing a single highly-ionizing track with stub and high $\not\!\!E_T$, so we looked in the data for single track events passing our Track, Stub, and Ionization cuts having $\not\!\!E_T < 20GeV$. We found 0 such events using our tight ionization cuts and also 0 events using our loose cuts. Using our fake rates from the jet sample calculated above, we would have expected many QCD events to populate this sample. The absence of such events shows that our factorized QCD Muon fake rates are overestimates. Therefore, in order to better pin down these fake rates, we will use this muon control sample for QCD Muon fake rate calculations. For the denominator of this fake rate, we counted the number of events in the muon data having only a base muon (with no additional base tracks) and $\not\!\!E_T < 20GeV$. Table 21 shows the numbers we obtained to calculate this fake rate.

Variable(s) cut	Cut value	# Passing	Loose/Tight QCD Muon fake rate (%)
single Base Muon	from Table 17, $\not\!\!E_T < 20GeV$	213,102	
Track, Stub, & Ion.	from Tables 1 & 3	0 (1 ± 1)	0.000469 ± 0.000469

Table 21: *$QCD \to H^{\pm\pm}$ Muon fake rates measured from low $\not\!\!E_T$, single-track muon sample with loose and tight ionization cuts. This fake rate, coupled with the QCD Track (loose and tight) fake rates from the jet samples is used in calculating the QCD background.*

6 Backgrounds

One advantage of performing a search for a long-lived doubly-charged particle is the lack of SM background. We expect the background to come in the form of highly ionizing muons, electrons, hadronic taus, and QCD jets as described in Section 5 above.

6.1 Muon Background

It is possible for only a Z event to produce these highly ionizing muons which make up the background for our study. Table 22 shows the expected number of muon background events. The background from muons would be proportional to the square of the muon fake rate (accounting for the duplicity of muons present, both of which must be fakes). Since cosmics are muon events and may be contained in this data sample, the background due to cosmics is also covered by this calculation.

	Loose Search	Tight Search
# $Z \to \mu\mu$ events	10,457	10,457
(μ Fake rate)^2	$(3.1 \pm 3.1(stat) \pm 0.6(syst)) \times 10^{-11}$	$(3.2 \pm 3.2(stat) \pm 0.5(syst)) \times 10^{-16}$
# μ Bkg. events	$(3.2 \pm 3.2(stat) \pm 0.6(syst)) \times 10^{-7}$	$(3.3 \pm 3.3(stat) \pm 0.5(syst)) \times 10^{-12}$

Table 22: *Long-lived doubly-charged Higgs background due to highly ionizing muons from Z's.*

6.2 Electron Background

It is also plausible for a Z event to produce electrons which are highly ionizing in both the tracking chamber and the calorimeters. Such an event would not only have to deposit a portion of it's energy in the electromagnetic calorimeter, but it would also need to slip through a crack in the detector and deposit energy in the hadronic calorimeter as well. The background calculation from electrons we present here employs the $e \to H^{\pm\pm}$ fake rate which we measured using $Z \to ee$ Monte-Carlo in Section 5.3. We rely on the correct modeling of the detector cracks in the simulation to give us an accurate background measurement.

In order to estimate the number of $Z \to ee$ background events, we perform a calculation as follows:

$$\begin{aligned} Z \to ee \text{ background} &= \left(n_1 \left(\frac{n_2}{n_3}\right)\left(\frac{\mathcal{L}_\mu}{\mathcal{L}_e}\right)\right) \times \left(e \text{ fake rate}\right)^2 \\ &= \left(\text{Est.}\#\ Z \to ee \text{ fakable events}\right) \times \left(e \text{ fake rate}\right)^2, \end{aligned} \tag{6}$$

where n_1 is the number of events in the $Z \rightarrow ee$ MC that passed the Track Cuts[4], n_2 and n_3 are the number of Z candidates in electron data and Z MC samples respectively, and $\mathcal{L}_\mu$ and $\mathcal{L}_e$ are the integrated luminosities of the respective data samples. Since there is a two-fold ambiguity of which electron fakes the tight muon, we multiply the result by a factor of 2.

Table 23 shows the values for these variables, and Table 24 shows the Z electron backgrounds derived using this method.

n_1	n_2	n_3	$\mathcal{L}_\mu$	$\mathcal{L}_e$
95,435	3,158	20,691	292.0 pb^{-1}	264.0 pb^{-1}

Table 23: *Values in Equation 6 that are used in calculating the estimated number of fakable electron events in the μ data sample.*

	Loose Search	Tight Search
Est.# $Z \rightarrow ee$ events	16,111	16,111
e (Muon × Track) Fake rate	$(3.0 \pm 3.0) \times 10^{-16}$	$(6.3 \pm 6.3) \times 10^{-19}$
# e Background events	$(9.6 \pm 9.6) \times 10^{-12}$	$(2.0 \pm 2.0) \times 10^{-14}$

Table 24: *Long-lived doubly-charged Higgs background due to highly ionizing electrons from Z's.*

6.3 Tau Background

A tau decaying hadronically could in theory have high enough ionization in the detector to pass the doubly charged Higgs ionization cuts and also punch through into the muon chamber. We calculate the background we should expect from this type of event using the tau fake rates we measured in Section 5.4.

We estimate the number of fakable tau events based on the number of $Z \rightarrow \mu\mu$ events we count in the data. Since this number can be corrected down based on muon inefficiency and up due to hadronic tau branching for the two τ's per event, we apply the following corrections to derive an estimated number of $Z \rightarrow \tau\tau$ events in the data:

$$\text{Est.\# } Z \rightarrow \tau\tau\text{'s} \quad = \quad \#Z \rightarrow \mu\mu \text{ events} \times \left(\frac{1}{\text{Measured } Z \rightarrow \mu\mu \text{ efficiency}} \right) \times \left(\begin{array}{c} \text{Branching ratio} \\ \geq 1 \text{ hadronic } \tau \end{array} \right)$$

[4]This is a separate MC sample (480,000 events from the `zewk1e` dataset) than that used for finding the electron fake rate in Table 13.

$$
\begin{aligned}
&= 10,457 \times \left(\frac{1}{0.832 \times 0.968}\right) \times \left(0.876\right) \\
&= 11,374 \text{ events,} \qquad (7)
\end{aligned}
$$

The backgrounds can be calculated directly from this estimated number of events, provided the fake rate applied is the product of the τ Track and Muon fake rates, since both a track and a stub are required in the search. As there is a two-fold ambiguity regarding which τ satisfies the tight muon requirements, we multiply the result by a factor of 2. These tau backgrounds are shown in Table 25.

	Loose Search	Tight Search
Est.# $Z \to \tau\tau$ events	11,374	11,374
τ (Muon $\times$ Track) Fake rate	$(3.2 \pm 3.2) \times 10^{-13}$	$(3.2 \pm 3.2) \times 10^{-13}$
# τ Background events	$(7.2 \pm 7.2 \times 10^{-9}$	$(7.2 \pm 7.2) \times 10^{-9}$

Table 25: *Long-lived doubly-charged Higgs background due to highly ionizing hadronic taus from Z's.*

6.4 QCD Background

We consider the case where unbiased jet events are misidentified as highly ionizing particles. We use the QCD Track and QCD Muon fake rates measured in Section 5.5. Recall that the we use the QCD Muon rates measured from the low-$\not\!\!E_T$ muon sample and the QCD Track rates from jet samples.

In order to find the QCD background contribution, we count the number of fakable QCD events using basic criteria. Fakable QCD events are defined as those events in our muon sample having both a base track and base muon (from Table 17). The number of background events from QCD can then be calculated by multiplying the number of fakable events by the product of the QCD Muon and QCD Track fake rates. The results of these QCD background calculations are shown in Table 26.

6.5 Total Background

The net background is found by adding the highly ionizing muon, electron, tau, and QCD backgrounds. Table 27 shows this calculation of the total background expected in the data for quasi-stable doubly-charged Higgs events.

	Loose Search	Tight Search
# fakable QCD events	19,198	19,198
QCD (Muon $\times$ Track) Fake rate	$(1.5 \pm 1.5(stat)^{+2.4}_{-1.3}(syst)) \times 10^{-9}$	$(1.3 \pm 1.3(stat)^{+0.2}_{-0.2}(syst)) \times 10^{-10}$
# QCD Background events	$(2.9 \pm 2.9^{+4.5}_{-2.6}) \times 10^{-5}$	$(2.5 \pm 2.5 \pm 0.4) \times 10^{-6}$

Table 26: *Long-lived doubly-charged Higgs background due to QCD.*

Background source	# Background Events in Loose Search	# Background Events in Tight Search
$Z \to \mu\mu$	$< 10^{-6}$	$< 10^{-11}$
$Z \to ee$	$< 10^{-11}$	$< 10^{-13}$
$Z \to \tau\tau$	$< 10^{-8}$	$< 10^{-8}$
QCD	$(2.9 \pm 2.9^{+4.5}_{-2.6}) \times 10^{-5}$	$(2.5 \pm 2.5 \pm 0.4) \times 10^{-6}$
All combined	$(2.9 \pm 2.9^{+4.5}_{-2.6}) \times 10^{-5}$	$(2.5 \pm 2.5 \pm 0.4) \times 10^{-6}$

Table 27: *Total background in both loose and tight search topologies from all potential sources for quasi-stable doubly-charged Higgs.*

7 Acceptance

We use 50,000 Monte-Carlo events generated with PYTHIA to determine the CDF Run II detector acceptance for finding doubly-charged Higgs particles. In order to properly simulate a quasi-stable, doubly-charged Higgs, something needs to be done to the particle when creating it in PYTHIA to prevent immediate decay. We generate H^{++}/H^{--} pairs having masses of 100 GeV, then immediately change their particle ID, mass, and energy to cause them to look like muons when passing through CDFSIM. In this way, we preserve the doubly-charged Higgs kinematics while allowing for stable particles. We also halve the momentum of each generated particle to account for it's doubled charge.

The kinematics of a $Z^0 \to H^{++}H^{--}$ event are quite different from that of a $Z^0 \to \mu\mu$ event. The large mass of the generated particles allows for a high generated p_T distribution, as can be seen in Figures 18 and 19. Figure 18 shows the apparent p_T distribution that the detector sees, and Figure 19 shows the true p_T of the doubly-charged Higgs.

The Higgs MC events are relatively slow as can be seen in the $\beta\gamma$ distributions at 100 and 160 GeV masses in Figure 20. Track reconstruction efficiency falls off gradually beginning with $\beta\gamma < 0.4$ due to failures in pattern recognition [12]. Fewer than 3.5% of our 160 GeV $H^{\pm\pm}$ (and fewer than 2% of 100 GeV ones) are slow enough to be in this lower-efficiency region, making the acceptance effect of slow Higgs only a fraction of a percent. This small effect is completely dominated by other systematic errors in the analysis.

Also, the doubly-charged Higgs events have a much narrower η spectrum compared to their muon counterparts in Figure 21. These two kinematic differences are instrumental in increasing the acceptance of the $Z^0 \to H^{++}H^{--}$ events. Since we use $Z^0 \to \mu\mu$ events in the calculation of our tracking efficiency, we show the η dependence of this efficiency in Figure 22. Since this figure is quite flat over the region of interest, we do not modify our efficiency based on the more narrow η values of the $H^{\pm\pm}$.

7.1 Measuring Doubly-Charged Higgs Acceptance

The kinematic and geometric cuts which we used in selecting our sample were as follows:

- z position of vertex $|z_0| < 60$ cm
- Reconstructed "muon" track with CMUP or CMX stub
  - COT exit radius $\rho_{COT} > 140$ cm
  - CMP/CMX fiducial "muon"
  - "Muon" track $p_T > 20$ GeV/c
- Second reconstructed "muon" track
  - COT exit radius $\rho_{COT} > 140$ cm
  - "Muon" track $p_T > 20$ GeV/c

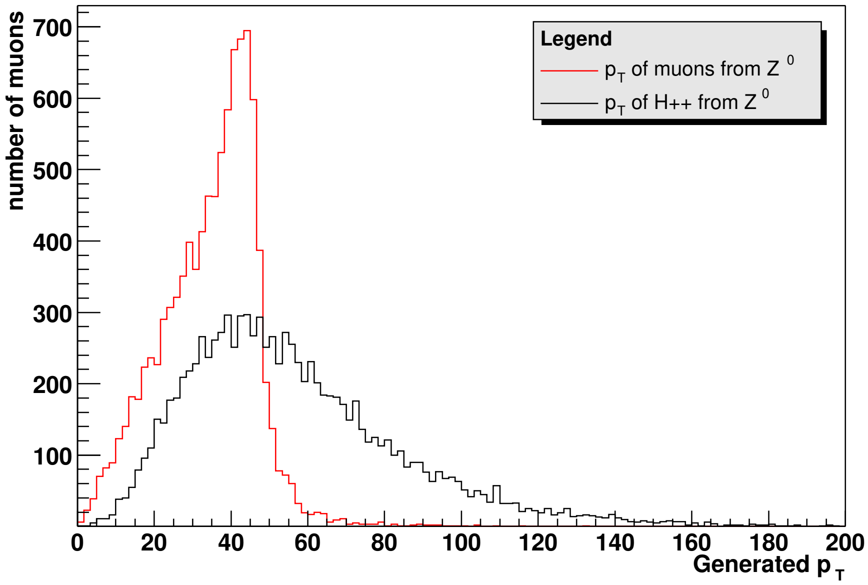

Figure 18: *The generator level p_T for muons from Z^0 and the apparent generator level p_T for 100 GeV doubly-charged Higgs from Z^0 as seen by the detector.*

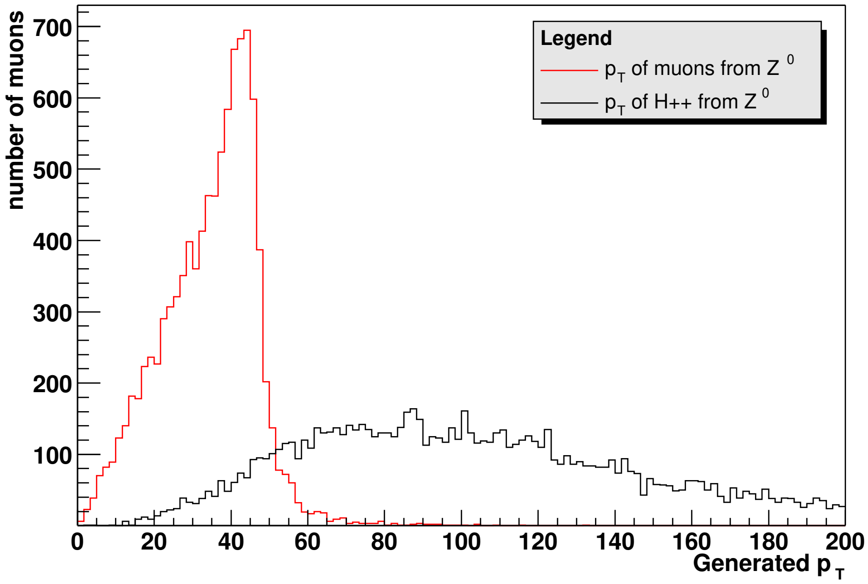

Figure 19: *The generator level p_T for muons from Z^0 and the true generator level p_T for 100 GeV doubly-charged Higgs from Z^0.*

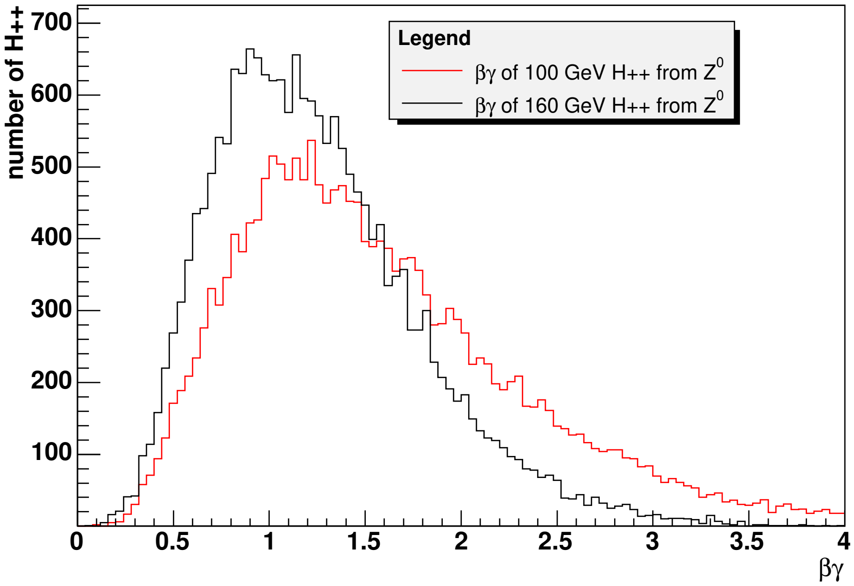

Figure 20: *The $\beta\gamma$ distributions from Monte Carlo of $Z^0 \rightarrow H^{++}H^{--}$ having masses of 100 and 160 GeV.*

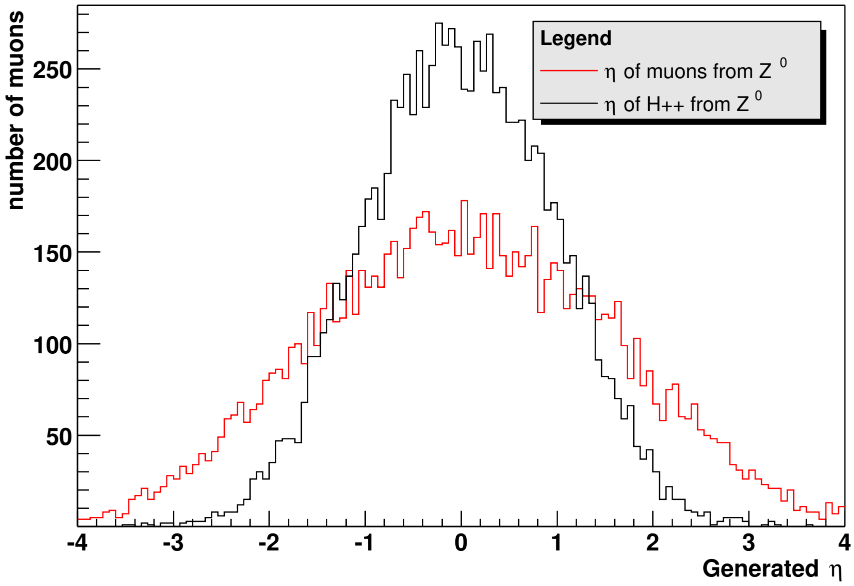

Figure 21: *The generated η distributions from Monte Carlo of $Z^0 \rightarrow H^{++}H^{--}$ and $Z^0 \rightarrow \mu\mu$.*

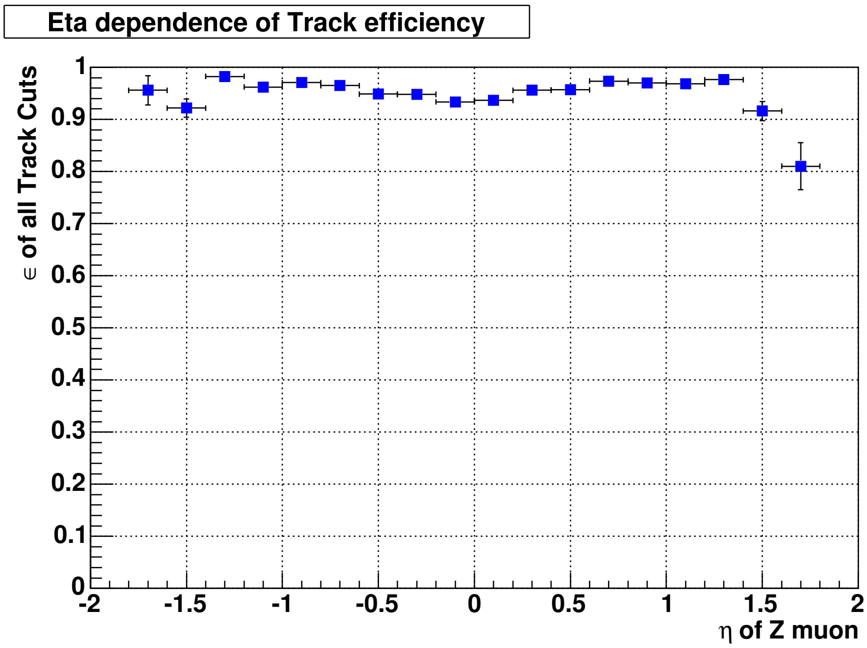

Figure 22: *The tracking efficiency as a function of η for $Z^0 \rightarrow \mu\mu$ data.*

These acceptance cuts are identical to the cuts used in calculating acceptance for Z's by the cross-section group in [13]. The ID cuts in Section 3 are not made when calculating the acceptance. It is to be interpreted as a pure geometric and kinematic acceptance. Table 28 and Figure 23 show the product of acceptance and efficiency for both the loose and tight topologies. The efficiencies listed are weighted to the distribution of events in the MC.

From these calculated acceptances, we can predict the number of $H^{\pm\pm}$ events we expect to see in the data. Table 29 shows these predictions at our four mass points.

8 Systematics

There are several sources of systematic uncertainties in the analysis. Here we measure the relative errors introduced by these uncertainties. We consider these sources: luminosity, K factor, PDF cross section, PDF acceptance, trigger efficiency, Z_{vtx} efficiency, ID efficiency, cosmic efficiency, energy scale, and energy resolution. Since all these sources of error contribute to the uncertainty applied to our Bayesian analysis, we list them here in one place. We find it necessary to point out though that both the K factor and PDF cross section errors correspond only to the theory cross-section and are not included with the others in the net systematic error on the experimental cross section.

$H^{\pm\pm}$ mass	Acceptance	Net Loose Efficiency	Loose Acc×Eff
90 GeV	0.3843 ± 0.0023	0.729 ± 0.092	0.280 ± 0.035
100 GeV	0.3951 ± 0.0023	0.728 ± 0.092	0.288 ± 0.036
130 GeV	0.4335 ± 0.0023	0.728 ± 0.092	0.316 ± 0.040
160 GeV	0.4681 ± 0.0023	0.728 ± 0.092	0.341 ± 0.043

$H^{\pm\pm}$ mass	Acceptance	Net Tight Efficiency	Tight Acc×Eff
90 GeV	0.3843 ± 0.0023	0.480 ± 0.061	0.184 ± 0.023
100 GeV	0.3951 ± 0.0023	0.479 ± 0.061	0.189 ± 0.024
130 GeV	0.4335 ± 0.0023	0.479 ± 0.061	0.208 ± 0.026
160 GeV	0.4681 ± 0.0023	0.479 ± 0.061	0.224 ± 0.029

Table 28: *Acceptances, net efficiencies, and their product for long-lived doubly-charged Higgs corresponding to either loose or tight search cuts having masses of 90, 100, 130, and 160 GeV respectively.*

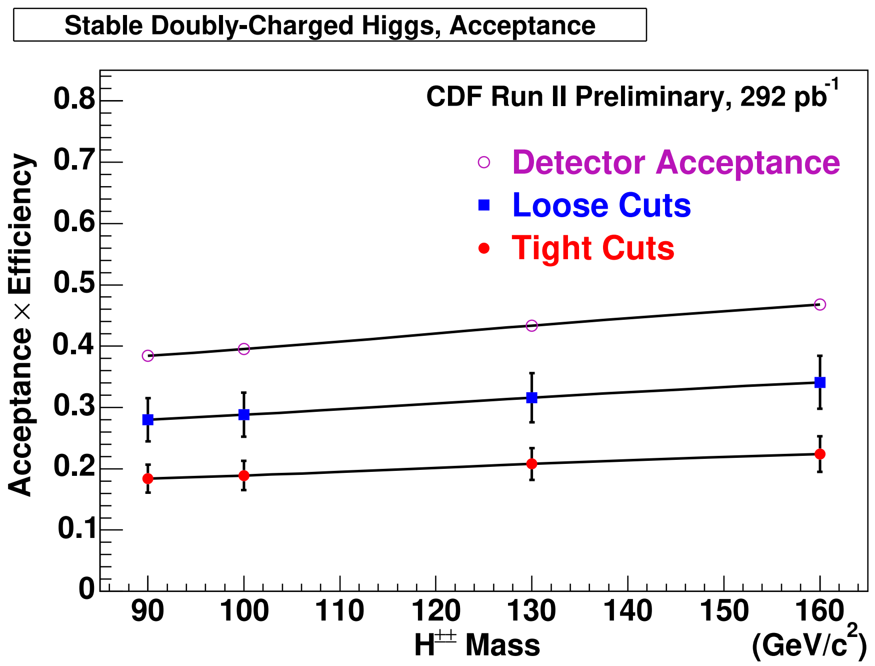

Figure 23: *Plot of the product of acceptance and efficiency corresponding to loose and tight ionization cuts. Also shown is the net fiducial and kinematic acceptance at various $H^{\pm\pm}$ masses before efficiencies are included.*

$H^{\pm\pm}$ mass	Loose $H^{\pm\pm}$ Events Expected	Tight $H^{\pm\pm}$ Events Expected
90 GeV	21.6 ± 3.5	14.2 ± 2.3
100 GeV	14.7 ± 2.4	9.6 ± 1.6
130 GeV	5.3 ± 0.8	3.5 ± 0.6
160 GeV	2.2 ± 0.4	1.4 ± 0.2

Table 29: *Number of stable doubly-charged Higgs expected in the data, corresponding to either loose or tight search cuts having masses of 90, 100, 130, and 160 GeV.*

8.1 Luminosity

The luminosity of our data sample with the run declared good for both the CMUP and CMX detectors is measured to be $292.0 \pm 16.6\ pb^{-1}$ [11]. The total uncertainty on this integrated luminosity is 6%, where 4.4% is from the acceptance and 4% is from the inelastic cross section [14].

8.2 K Factor

The theoretical cross sections at next-to-leading-order (NLO) for the doubly charged Higgs contain systematic errors based on the uncertainty in the K factor. These errors coming from renormalization and factorization scale dependence were estimated at the time of their calculation to be between $5-10\%$ [16]. For our systematic error, we take the central value in the stated range, 7.5%.

8.3 PDF Cross Section

The uncertainty on the cross-section results from the parton distribution function (PDF). We chose to use CTEQ6L as the PDF for our central value. We investigate the effect of different PDF choices by folding in the cross section errors from the 40 alternate eigenvectors in CTEQ6 following the EWK prescription [15]. We generate 100,000 events for each of the 41 PDF's at each of our mass points. The systematic errors for each mass point are shown in Table 30.

8.4 PDF Acceptance

The acceptance also depends on the kinematic and fiducial acceptance of the chosen PDF. To calculate this error, we find the generator level acceptance of the 100,000 events generated above for each mass point and eigenvector. We again follow the EWK prescription for calculating the acceptance uncertainty due to PDF's and list the errors we find in Table 30.

8.5 Trigger & Stub Efficiency

The trigger and stub efficiencies for the triggers used in our analysis (MUON_CMUP_18 and MUON_CMX_18) were weighted to the fiducial distribution of $H^{\pm\pm}$ MC in Table 9. Our net trigger efficiencies for $H^{\pm\pm}$ having masses of 90, 100, 130, and 160 GeV were 0.965 ± 0.007, 0.964 ± 0.007, 0.963 ± 0.006, and 0.964 ± 0.006 respectively. These translate to systematic errors on the acceptance of 0.73%, 0.73%, 0.62%, and 0.62% at the four mass values.

8.6 Z_{vtx} Efficiency

The Z vertex efficiency has been measured to be $.950 \pm 0.004$ [13]. From this measurement we calculate the relative systematic error on the net acceptance to be 0.42% for all mass points considered.

8.7 Identification Efficiency

The ID efficiency (excluding the Z vertex efficiency shown above) is calculated to be 0.504 ± 0.062 from its three remaining components in Table 8. Each of the three efficiencies comprising this ID efficiency were found by squaring the efficiency for a single particle to pass the cut. This results in a systematic error on the acceptance of 10.7%.

8.8 Cosmic Efficiency

The upper bound on the inefficiency of the cosmic tagger used has been measured to be 0.8% [11]. This bound can be used to estimate a systematic uncertainty for the cosmic-rejection algorithm on the acceptance of doubly-charged Higgs events.

8.9 Energy Scale

To find the systematic error due to energy scale uncertainty, we began by finding the dimuon mass distribution for $Z \to \mu\mu$ candidates in the data compared to simulated $Z \to \mu\mu$ events. Fitting a gaussian to this distribution between 82 and 100 GeV, we found the mean value for the Z mass peak to be 90.782 ± 0.054 GeV for data candidates and 90.887 ± 0.021 GeV for MC events. Thus, we applied a scale factor of 0.9988 to the simulated energies which resulted in a scaled Z mass peak of 90.782 ± 0.021 GeV for MC events. We measure what change in the energy scale factor would be needed to shift the Z mass peak in the simulation by twice the statistical error on the mean mass in the data ($0.054 \times 2 = 0.108$). Scaling the energies by $\pm 0.125\%$ is found to accomplish this, so we include this additional scale factor in the MC energies to determine the effect of the energy scale errors on the acceptance. We recalculate our acceptances with this additional shift of $\pm 0.125\%$ on the energies. Since this energy scale spread corresponds to a shift of four standard deviations, we divide the net change in acceptance by 4 to find the error this uncertainty contributes. The contributed systematic error at each mass can be seen in Table 30.

8.10 Energy Resolution

The systematic error due to energy resolution uncertainty is derived in much the same way as energy scale above. Now, instead of scaling the mean of the Z peak so the simulation matches the data, we apply a gaussian smear so the RMS widths are the same. A gaussian fitted to the Z mass peak between 82 and 100 GeV had an RMS width of 3.81 ± 0.05 GeV in the data and 3.28 ± 0.02 GeV in the simulation. We found that smearing the energies in the simulation by 1.90% increased its RMS width to 3.80 ± 0.02, thus matching the data width to well within the statistical errors. We find the necessary change in the energy smearing to increase or decrease the MC width by twice the statistical error on the data ($0.05 \times 2 = 0.10$). Smearing the energies by $\pm 0.35\%$ increases and decreases the simulation width by these 2 standard deviations, so we apply this additional smearing factor to the $H^{\pm\pm}$ MC to determine its effect on the acceptances. We divide the net change in acceptance for each mass point by 4, since four standard deviations separate the two values and include the resulting uncertainty on the acceptance in Table 30.

8.11 Systematic Summary

Table 30 summarizes all uncertainty contributions resulting from each source of error at our three mass values. We add the individual errors in quadrature to determine the total systematic error for each mass point. The net systematic errors include errors to both the experimental and theoretical cross sections. While we realize that the theoretical errors are not a part of the experimental cross sections, we combine them as such so the Bayesian analysis to follow can incorporate as many of the errors as possible in its single error input. Table 31 shows the separation of these errors to the respective cross sections, both experimental and theoretical.

9 Results

We observe no doubly-charged two-track events passing either the loose or tight ionization cuts. We use this lack of evidence for stable doubly-charged particles to set limits on long-lived doubly-charged Higgs pair production.

To set a limit on the mass of the $H^{\pm\pm}$ we have chosen *apriori* to use our loose ionization cuts to determine the experimental cross section. We use a Bayesian approach for this process [17]. After entering the total background expected for our signal, the error on that background, and a 15.7% error on the acceptance (mean value for the three high mass points), the "bayes.f" program (provided by the CDF Statistics Group) returned a value of < 3.211 signal events at a 95% C.L. for 0 events observed. This permitted us to find the experimental cross section for each doubly-charged Higgs mass when put into the following equation:

$$\sigma_{exp}(M_H) \;=\; \frac{\#\text{ signal events}}{luminosity \times \text{``}Loose\ Acc \times Eff\text{''}(M_H)}$$

Systematic	90 GeV $H^{\pm\pm}$	100 GeV $H^{\pm\pm}$	130 GeV $H^{\pm\pm}$	160 GeV $H^{\pm\pm}$
Luminosity	6	6	6	6
K factor	7.5	7.5	7.5	7.5
σ_{PDF}	4.49	4.80	5.06	5.55
PDF acc.	1.15	1.13	0.98	0.95
Trigger eff.	0.73	0.73	0.62	0.62
Z_{vtx} eff.	0.42	0.42	0.42	0.42
ID eff.	10.7	10.7	10.7	10.7
Cosmic eff.	0.8	0.8	0.8	0.8
E scale	0.006	0.0005	0.0005	0.0005
E resolution	0.005	0.004	0.0006	0.001
Total	15.5	15.6	15.7	15.8

Table 30: *Summary of all systematic uncertainties. Errors shown are relative errors in percentages. Total errors for each mass point were found by adding the individual errors in quadrature for the corresponding mass, except for σ_{PDF} and PDF acceptance which are expected to be correlated so were added linearly. These totals are the cumulative theoretical and experimental errors used in our Bayesian analysis.*

$$= \frac{3.211}{(292.0 \pm 16.6)\, pb^{-1} \times \text{“}Loose\ Acc \times Eff\text{''}(M_H)}. \tag{8}$$

From this equation we received four experimental cross-section limits for Higgs masses of 90, 100, 130, and 160 GeV shown in Table 31. Since we expected only negligible background, our *apriori* expected limit plot is identical to the limit plot from the data. The data result in a lower mass limit of 146 GeV for long-lived $H^{\pm\pm}$ in all decay channels. We use the next to leading order theoretical cross sections at each respective mass.

$H^{\pm\pm}$ mass	Loose Acc×Eff	Experimental Limit σ (pb)	Theoretical σ_{NLO} (pb)
90 GeV	$0.280 \pm .035$	0.0393	$0.26443 \pm .02311(syst)$
100 GeV	$0.288 \pm .036$	0.0382	$0.17435 \pm .01553(syst)$
130 GeV	$0.316 \pm .040$	0.0348	$0.05783 \pm .00523(syst)$
160 GeV	$0.341 \pm .043$	0.0322	$0.02186 \pm .00204(syst)$

Table 31: *Cross section limits for long-lived doubly-charged Higgs at the mass values of 90, 100, 130, and 160 GeV.*

Figure 24 illustrates the mass limit set by this analysis by showing where the curves created by our theoretical and experimental cross sections intersect.

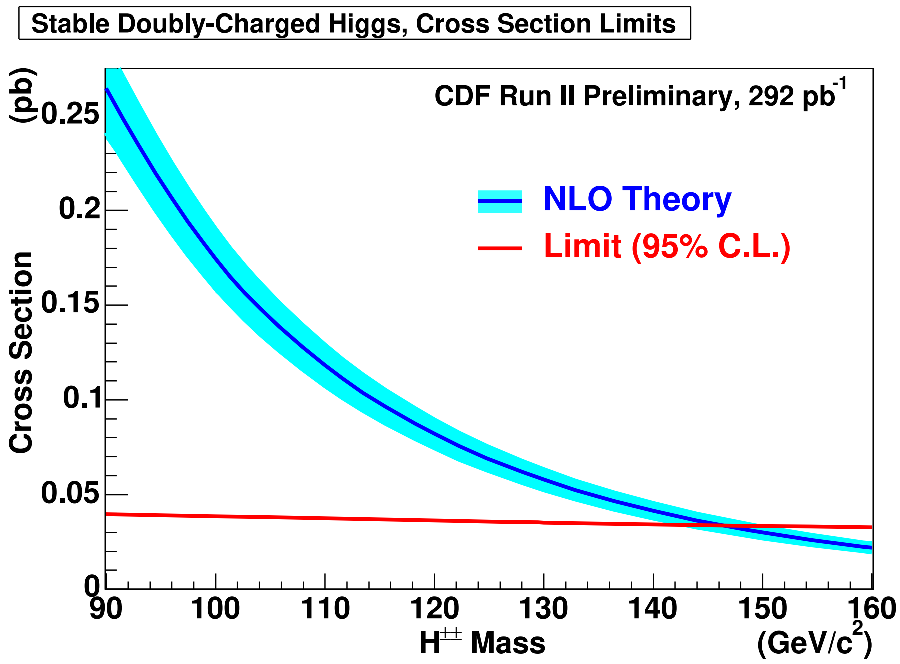

Figure 24: *The theoretical and experimental $H^{\pm\pm}$ cross section limits for the loose ionization cuts. The intersection corresponds to a long-lived doubly-charged Higgs mass limit for the analysis of 146 GeV.*

References

[1] C. Hays and A. Kotwal, *CDF Note* **6342** (2003).

[2] C. Hays and A. Kotwal, *CDF Note* **6457** (2003).

[3] C. Hays and A. Kotwal, *CDF Note* **6604** (2003).

[4] J. Tuttle *et al. CDF Note 6856* (2004).

[5] J. Tuttle *et al. CDF Note 7050* (2004).

[6] Private communication with Oliver Stelzer-Chilton *(oliver@physics.utoronto.ca)* (2004).

[7] D. E. Groom *et al. Eur. Phys. J.,* **C15** ,1 (2000).

[8] S. Yu *et al. CDF Note* **6361** (2003).

[9] G. Punzi, D. Tonelli, *et al. CDF Note* **6932** (2004).

[10] H. Gerberich *et al. CDF Note* **6089** (2002).

[11] C. Hays and A. Kotwal, *CDF Note* **6833** (2004).

[12] W. Orejudos and F.D. Snyder, *CDF Note* **6307** ver.2.1 (2003).

[13] D. Amidei *et al.* *CDF Note* **6711** ver.3 (2003).

[14] S. Klimenko *et al.* *CDF Note* **6314** (2004).

[15] The EWK prescription for determining PDF uncertainty can be found in this talk: http://www-cdf.fnal.gov/internal/WebTalks/0404/links/040402_joint_physics_Tony_1_JointPhys_040204.pdf.

[16] M. Muhlleitner and M. Spira, *Phys. Rev. D.,* **68** ,117701 (2003).

[17] The Fortran code from the CDF Statistics group for calculating the Bayesian probability can be found at http://www-cdf-fnal.gov/physics/statistics/code/bayes.f.